



National Library
of Canada

Acquisitions and
Bibliographic Services Branch

395 Wellington Street
Ottawa, Ontario
K1A 0N4

Bibliothèque nationale
du Canada

Direction des acquisitions et
des services bibliographiques

395, rue Wellington
Ottawa (Ontario)
K1A 0N4

Your file - Votre référence

Our file - Notre référence

NOTICE

The quality of this microform is heavily dependent upon the quality of the original thesis submitted for microfilming. Every effort has been made to ensure the highest quality of reproduction possible.

If pages are missing, contact the university which granted the degree.

Some pages may have indistinct print especially if the original pages were typed with a poor typewriter ribbon or if the university sent us an inferior photocopy.

Reproduction in full or in part of this microform is governed by the Canadian Copyright Act, R.S.C. 1970, c. C-30, and subsequent amendments.

AVIS

La qualité de cette microforme dépend grandement de la qualité de la thèse soumise au microfilmage. Nous avons tout fait pour assurer une qualité supérieure de reproduction.

S'il manque des pages, veuillez communiquer avec l'université qui a conféré le grade.

La qualité d'impression de certaines pages peut laisser à désirer, surtout si les pages originales ont été dactylographiées à l'aide d'un ruban usé ou si l'université nous a fait parvenir une photocopie de qualité inférieure.

La reproduction, même partielle, de cette microforme est soumise à la Loi canadienne sur le droit d'auteur, SRC 1970, c. C-30, et ses amendements subséquents.

Canada

University of Alberta

**ANALYSIS OF EROSION IN A CONTROL VALVE
DUE TO SOLID PARTICLES**

by

Bernard V. Stadlwieser



A thesis submitted to the Faculty of Graduate Studies and Research in partial fulfillment of the requirements for the degree of **Master of Science**.

Department of Mechanical Engineering

Edmonton, Alberta
Fall 1994



National Library
of Canada

Acquisitions and
Bibliographic Services Branch

395 Wellington Street
Ottawa, Ontario
K1A 0N4

Bibliothèque nationale
du Canada

Direction des acquisitions et
des services bibliographiques

395, rue Wellington
Ottawa (Ontario)
K1A 0N4

Acquis - Acquisitions

Collection - Notre collection

The author has granted an irrevocable non-exclusive licence allowing the National Library of Canada to reproduce, loan, distribute or sell copies of his/her thesis by any means and in any form or format, making this thesis available to interested persons.

L'auteur a accordé une licence irrévocable et non exclusive permettant à la Bibliothèque nationale du Canada de reproduire, prêter, distribuer ou vendre des copies de sa thèse de quelque manière et sous quelque forme que ce soit pour mettre des exemplaires de cette thèse à la disposition des personnes intéressées.

The author retains ownership of the copyright in his/her thesis. Neither the thesis nor substantial extracts from it may be printed or otherwise reproduced without his/her permission.

L'auteur conserve la propriété du droit d'auteur qui protège sa thèse. Ni la thèse ni des extraits substantiels de celle-ci ne doivent être imprimés ou autrement reproduits sans son autorisation.

ISBN 0-315-95115-X

Canada

University of Alberta

Release Form

Name of Author: Bernard Vincent Stadlwieser

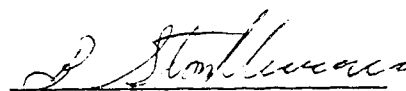
Title of Thesis: ANALYSIS OF EROSION IN A CONTROL VALVE
DUE TO SOLID PARTICLES

Degree: Master of Science

Year this degree granted: Fall 1994

Permission is hereby granted to **The University of Alberta Library** to reproduce single copies of this thesis and to lend or sell copies for private, scholarly or scientific research purposes only.

The author reserves all other publication and other rights in association with the copyright in the thesis, and except as hereinbefore provided neither the thesis nor any substantial portion thereof may be printed or otherwise reproduced in any material form whatever without the authors's prior written permission.



Bernard V. Stadlwieser

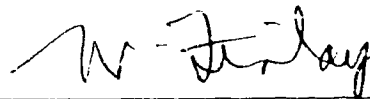
R.R.1.South Edmonton
Edmonton, Alberta
T6H 4N6

Date: August 29, 1994

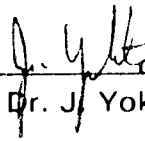
University of Alberta

Faculty of Graduate Studies and Research

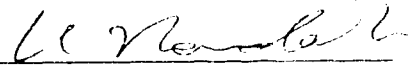
The undersigned certify that they have read, and recommended to the Faculty of Graduate Studies and Research for acceptance, a thesis entitled **ANALYSIS OF EROSION IN A CONTROL VALVE DUE TO SOLID PARTICLES** submitted by **Bernard V. Stadlwieser** in partial fulfillment of the requirements for the degree of **Master of Science**.



Dr. W. H. Finlay



Dr. J. Yokota



Dr. K. Nandakumar

Date: August 26, 1994

To My Parents

Abstract

An analysis of erosion caused by sand & clay particles entrained in a hydrocarbon flow through a high pressure letdown valve is discussed.

In order to model the erosion of the valve surfaces, the flow field and particle trajectories were obtained in the complex valve geometry. The commercial package CFDS-FLOW3D was used for this purpose. FLOW3D uses a finite volume formulation with a non-orthogonal body-fitted structured grid, and a pressure correction method. The turbulence was modelled with a $k-\epsilon$ turbulence model. The simulation assumed a dilute fluid-particle flow. The particle phase was modelled with a Lagrangian approach. Having obtained particle impingement locations, velocities, and angles, the erosion caused by impinging particles was modelled by empirical wear models. For ductile materials we use Finnie's cutting erosion model and Hutchings fatigue erosion model, while for the brittle materials of the valve we use Evans, Gulden and Rosenblatt's Elastic-Plastic erosion model.

When compared to the wear patterns of the operational valve, the results show that the erosion can be predicted qualitatively. Quantitative agreement was not possible because of the many assumptions needed to make the problem tractable. The assumptions of no fluid-particle, particle-particle interactions, and the lack of understanding of the particle-material wear interactions are the most severe assumptions. Experimental verification of the flow field and particle trajectories was not possible and with such a complex geometry inaccuracies are certain to occur.

ACKNOWLEDGEMENT

The author would like to take this opportunity to express his deepest appreciation to the people who contributed their valuable time, advice and resources towards this thesis.

These distinct individuals are as follows:

Dr. W. H. Finlay for his valuable advice, guidance and encouragement.

Mr. L. P. Hackman for his valuable advice and support.

Mr. C. J. Horvath for information on the operational valve.

Table of Contents

Chapter 1	1
Chapter 2	3
2.1 Fluid Flow Field Modelling in the Valve	3
2.1.1 <i>Solution Methods for Transport Equations</i>	3
2.1.2 <i>Fluid Assumptions for the Valve simulation</i>	5
2.1.3 <i>Boundary Conditions of the Valve</i>	5
2.2 Solution Method for Particle Trajectories in the Valve	6
2.2.1 <i>Solution Method for Equations of Motion</i>	6
2.2.2 <i>Modifications to FLOW3D to Model Particles Impacts</i>	8
2.2.3 <i>Inlet Conditions in the Valve for Particle Trajectories</i>	8
Chapter 3	12
3.1 Governing Particle Properties in Solid Particle Erosion	12
3.2 Surface Effects of Solid Particle Erosion	13
3.3 Corrosion Effects on Erosion	14
3.4 Erosion Modelling of Steel Parts in the Valve	15
3.5 Erosion Modelling of WC-Co Parts of the Valve	18
Chapter 4	22
4.1 Flow Field	22
4.1.1 <i>Grid Independence of the Flow Field</i>	22
4.1.2 <i>Analysis of the Flow Field in the Valve</i>	23
4.2 Particle Trajectories Through the Valve	25
4.2.1 <i>Particle Impact Results</i>	25
4.2.2 <i>Effect of Turbulent Dispersion</i>	28
4.2.3 <i>FLOW3D Particle Tracking Problems</i>	28

4.3 Comparison of Simulated to Operational Wear Patterns	29
Chapter 5	50
5.1 <i>Conclusions</i>	50
5.2 <i>Suggestions for Further Work</i>	51
References	53

List of Figures

Figure 2.1.	Valve cross section with labelled valve parts.	10
Figure 2.2.	Cross section of multi-block structure.	11
Figure 3.1.	Schematic representation of erosion rate against impact angle. . .	21
Figure 4.1.	Effect of grid refinement on flow characteristics in the valve tip region.	33
Figure 4.2.	Effect of grid refinement on flow characteristics at the bottom of valve seat rings.	34
Figure 4.3.	Cross section of flow field in main body of valve.	35
Figure 4.4.	Cross section of flow field in valve seat rings.	36
Figure 4.5.	A comparison of measured flow coefficients to the simulated . . . flow coefficients with percentage of valve travel.	37
Figure 4.6.	Comparison of particle trajectory with particle size.	38
Figure 4.7.	Averaged particle impact results for 10 μm particles on the interior valve surfaces plotted in the streamwise direction.	39
Figure 4.8.	Averaged particle impact results for 10 μm particles on the valve plug surfaces plotted in the streamwise direction.	39
Figure 4.9.	Particle impact results for 20 μm particles on the	40
	interior valve surfaces.	
Figure 4.10.	Particle impact results for 20 μm particles on the	41
	valve plug surfaces.	
Figure 4.11.	Particle impact results for 50 μm particles on the	42
	interior valve surfaces.	
Figure 4.12.	Particle impact results for 50 μm particles on the	43
	valve plug surfaces.	
Figure 4.13.	Averaged particle impact results for 100 μm particles on the . . . interior valve surfaces plotted in the streamwise direction.	44

Figure 4.14.	Averaged particle impact results for 100 μm particles on the valve plug surfaces plotted in the streamwise direction.	44
Figure 4.15.	Particle trajectories with and without turbulent dispersion for 10 μm particles.	45
Figure 4.16.	Comparison between predicted and actual wear patterns for the valve's main body.	46
Figure 4.17	Comparison between predicted and actual wear patterns for the valve seat rings.	47
Figure 4.18	Comparison between predicted and actual wear patterns for the valve plug assembly.	48
Figure 4.19.	Schematic representation of erosion predominantly to one side of the seat rings.	49
Figure 4.20.	Schematic representation of erosion predominantly to one side of the valve tip.	49

Symbols and Nomenclature

C	Constant in erosion models
C_{p1}	Empirical constant for turbulent kinetic energy
C_{p2}	Empirical constant for turbulent dissipation rate
C_v	Flow coefficient
D	Hydraulic diameter
D_m	Density of WC-Co
D_p	Density of the particle
DP	Pressure drop
d_p	Diameter of the particle
e	Coefficient of restitution
E_{max}	Maximum erosion rate used to non-dimensionalize results
ϵ	Turbulent dissipation rate
H	Dynamic hardness of WC-Co
k	Turbulent kinetic energy
K_f	Constant for Hutchings model accounting for dynamic hardness and erosion ductility
K_c	Dynamic toughness of WC-Co
L_c	Characteristic length scale
μ	Viscosity
M_p	Mass of particle
P	Constant in Finnie's model accounting for dynamic hardness

Q	Fluid flowrate
R_p	Radius of the particle
SPG	Specific gravity of fluid
S_t	Stokes Number
θ	Impact angle of particle
τ_f	Flow field time scale
τ_p	Particle relaxation time factor
U_c	Characteristic velocity
U_{cr}	Critical velocity
U_m	Mean velocity
U_p	Impact velocity of particle
V	Volume removed by impacting particles
V_{N1}	Normal component of velocity before impact
V_{N2}	Normal component of velocity after impact

Chapter 1

Synchrude Canada Ltd. operates the largest synthetic crude oil production facility in the world. The bitumen feedstock is processed by an ebullated bed hydrocracker (LC-Finer) unit to produce synthetic crude. The synthetic crude from the LC-Finer unit contains approximately one percent solids by mass. The passage of this material through the high pressure letdown valve at the exit of the LC-Finer results in significant erosion of the letdown valve. The continuous failure of this large control valve by solid particle erosion was simulated in this study, and the failure information was compared with the results of the simulation. This valve is a critical control valve, and insight into solid particle erosion of the valve could increase valve reliability and reduce costs such as lost production and replacement of expensive valves and valve trims.

With the advancement of computational fluid dynamics and computers a numerical simulation of erosion in the valve is possible. The three necessary steps to model the erosion include simulating the flow field, calculating the particle trajectories, and modelling the erosion caused by particle impacts at walls. To the author's knowledge, the first study incorporating these three aspects into erosion estimation was developed for gas turbines at the University of Cincinnati by Grant and Tabakoff¹, and Beacher, Tabakoff, and Hamed². A number of other researchers have also studied erosion in this manner: Benim and Neuhoff³ simulated erosion in turbocharger radial turbines using CFDS-FLOW3D, Ahmad and Goulas⁴ simulated erosion in slurry pumps, Nesic and

Postlethwaite⁵ simulated erosion-corrosion in sudden pipe expansions, Benchatia et al⁶ simulated erosion in channel bends, and Humphrey et al⁷ modelled the influence of turbulence on erosion by particle-laden fluid jets. These simulations were able to qualitatively predict erosion prone areas in the particular application studied. A flow simulation through Poppet Valves by Vaughan et al⁸ was qualitatively able to predict the flow patterns. The present study simulates the full three dimensional flow field and the particle trajectories in Syncrude's LC-Finer control valve and uses empirical wear models to simulate the three dimensional wear pattern of this valve.

Chapter 2

2.1 Fluid Flow Field Modelling in the Valve

2.1.1 Solution Method for Transport Equations

The transport equations for the fluid phase were solved using the commercial computational fluid dynamics package CFDS-FLOW3D. FLOW3D uses a finite volume formulation with a non-orthogonal body fitted structure grid, and the SIMPLEC pressure correction method. Turbulence was modelled with the $k-\epsilon$ turbulence model. The Hybrid differencing scheme was used for differencing; if the Peclet Number is less than two then central differencing is used, otherwise upwind differencing is used.

The valve was meshed as a full three dimensional model; the mesh generation package Sophia of CFDS-FLOW3D was used to construct the complex geometry. Figure 2.1 provides a cross section of the complex valve geometry, and different parts of the valve are displayed in the figure. This valve consists of six parts in the flow cavity; these are the main body with two seat rings which have Tungsten Carbide (WC-Co) inserts, the valve liner, the valve stem, and a WC-Co valve tip. The valve was divided into either 58 or 66 block structures, most of which have curved edges as shown in figure 2.2. An elliptic iterative technique was used to generate the mesh which is well suited for curved surfaces. At the outlet of the valve an additional three diameters of pipe was added as

shown in figure 2.2 to minimize the upstream influence of the computational outlet boundary. On site the constant diameter pipe downstream of the valve extends for approximately four more meters. At the inlet a straight section of pipe also precedes the valve, but this and a small straight section of the valve's inlet was neglected in order to reduce the number of cells. The effect of neglecting this straight section on the flow field was minimized by inputting a fully developed turbulent velocity profile for a pipe at the inlet. Several grids were used having either 51,860; 95,856; 168,364; 240,128; (58 blocks) or 135,000 cells (66 blocks). Computational times to reach a converged solution typically exceeded one week on a IBM RS6000/560 and required up to 385 mega bytes random access memory; these requirements make this type of simulation costly and time consuming.

In order to obtain a converged solution, it was necessary to use false-time steps and double precision. Initial small false-time steps, of order 10^{-5} seconds allowed for the establishment of a reasonable flow pattern after which the false-time steps could be raised to increase the convergence rate. The cross-derivative diffusion terms in the $k-\epsilon$ equations can cause rapid divergence; this is due to extremely small values of ϵ which result in a large eddy viscosity, which is not physically possible. These terms can initially be omitted from the $k-\epsilon$ equations until a sensible flow pattern has been established and then included. For more details refer to the CFDS-FLOW3D user manual 3.2⁹.

2.1.2 Fluid Assumptions for the Valve Simulation

The fluid flowing through the valve was assumed to be a single phase incompressible Newtonian hydrocarbon. The flow was assumed to be at steady state and to be isothermal. The viscosity of the fluid is $3.5(10^{-4})$ Pa/s and the density is 703 Kg/m^3 at the operational temperature of 440° C , these values were obtained from measurements by Syncrude.

2.1.3 Boundary Conditions of the Valve

The flowrate through the valve is $7153 \text{ m}^3/\text{day}$ at a valve setting of 43% of the valve's full stroke of 28.62mm. This setting was determined from the valve manufactures flow coefficients and the operational valve. A fully developed turbulent pipe velocity profile with a $1/7$ power law was assumed for the inlet velocity, and the user fortran routine "usrbcs.f" was modified to input the profile. The turbulent kinetic energy and dissipation rate were scaled to the mean inlet velocity with the following equations obtained from the CFDS-FLOW3D user manual 3.2⁹.

$$k \approx C_{p1} U_m^2 \quad (1)$$

$$\epsilon \approx \frac{k^{1.5}}{C_{p2} D} \quad (2)$$

Here, the values of the empirical constants C_{p1} and C_{p2} are 0.002 and 0.3 respectively. Neumann boundary conditions were applied at the outlet of the valve. No slip boundary conditions were applied to the walls of the valve.

2.2 Solution Method for Particle Trajectories in the Valve

2.2.1 Solution Method for Equations of Motion

Particle trajectories were modelled using a Lagrangian approach, and this was done by using the particle tracking routines of CFDS-FLOW3D. A good review of solid particle erosion by Humphrey¹⁰ indicates that modelling the particle trajectories in this manner is only valid if the system is dilute, with mass fractions of less than roughly one percent. In this study the mass fraction of solid particles was approximately one percent.

The main forces acting on the particles are the hydrodynamic drag force due to the mean flow field, the pressure gradient force, and turbulent dispersion due to the fluctuating component of the turbulent flow. The drag force is simply the force exerted on the particles by the mean component of the continuous phase. The pressure gradient force was included because of the relatively small ratio of 3.75 between the particle and fluid density, and because of the high pressure gradients in the valve. Turbulent dispersion adds irregular motion to the particles causing them to impact walls more frequently and be ejected from boundary layers. Turbulent dispersion substantially increased the number of impacts when compared to it being neglected.

The force due to buoyancy is neglected since the ratio of particle and fluid density was 3.75 and the settling velocities are orders of magnitude smaller than the particle impact velocity which is a measure of relative velocity between the fluid and the particles near the valve surfaces. Additional forces which were neglected are the Saffman, Magnus, lift, and particle-particle interactions, since these forces are relatively small and also to keep the calculation of particle trajectories tractable. The relative magnitudes of these forces is discussed in a good review by Humphrey¹⁰.

How a particle rebounds after impacting a surface can have a major impact on erosion. For this simulation a simple coefficient of restitution ($V_{N2} = -eV_{N1}$) was used, and a value of e was taken as 0.8. This value allowed for a reasonable simulation of the particle impacts, while reducing particle tracking difficulties due to slow moving particles along valve surfaces. These slow moving particles do not advance in space and therefore cannot be tracked through the complete valve. Experimental data correlations such as those done by Tabakoff et al² and Ottjes¹¹ were not possible, since no experimental rebound characteristic information is available for the particles and materials used in the present study.

For more details refer to the CFDS-FLOW3D User Manual 3.2⁹.

2.2.2 Modifications to FLOW3D to Model Particle Impacts

Two of the parameters required from the particle trajectories, impact location and velocity, are readily available in the standard CFDS-FLOW3D routines. The final parameter of impact angle can be obtained from the routine "bcspar.f" by using the parallel and perpendicular components of velocity at the point of impact. The impact location, velocity, and angle were written to a file by modifying the subroutines "track.f" and "printd.f". In order to limit the size of the impact information file particle impact information was only written if the particle advanced 0.75 mm in space.

The user fortran routine "usrpbc.f" was modified to read in a file of initial starting locations for the particles. The input file of starting locations was generated by running an initial run with a modified user routine "usrint.f" which has access to the cell vertex arrays. This allows a real space location to be translated into computational space where the particles are tracked.

2.2.3 Inlet Conditions in the Valve for Particle Trajectories

Across the inlet of the valve the particles were equally spaced every 0.8 mm with no particle within 1 mm of the inlet walls. This resulted in 6073 particles being tracked through the valve. Each particle represented a mass flux of $9.55(10^{-5})$ Kg/s starting from that location, resulting in a total solids flowrate of 0.58 Kg/s, which is representative of

that seen on site.

Four different sizes of monodisperse particles were simulated including 10, 20, 50, and 100 μm particles. Work done by Stropki^{12,13} for Syncrude indicates that the mean particle size is between 10-20 μm , but operational changes and plant upsets may cause size variations. The inlet velocity of all the particles was set to the mean inlet velocity of 12.44 m/s in order to limit interpolation for velocities for each starting location. The particles were assumed to be spherical clay and sand particles with a density of 2600 Kg/m^3 . The particles were tracked through the 168,364 and 135,000 cell meshes.

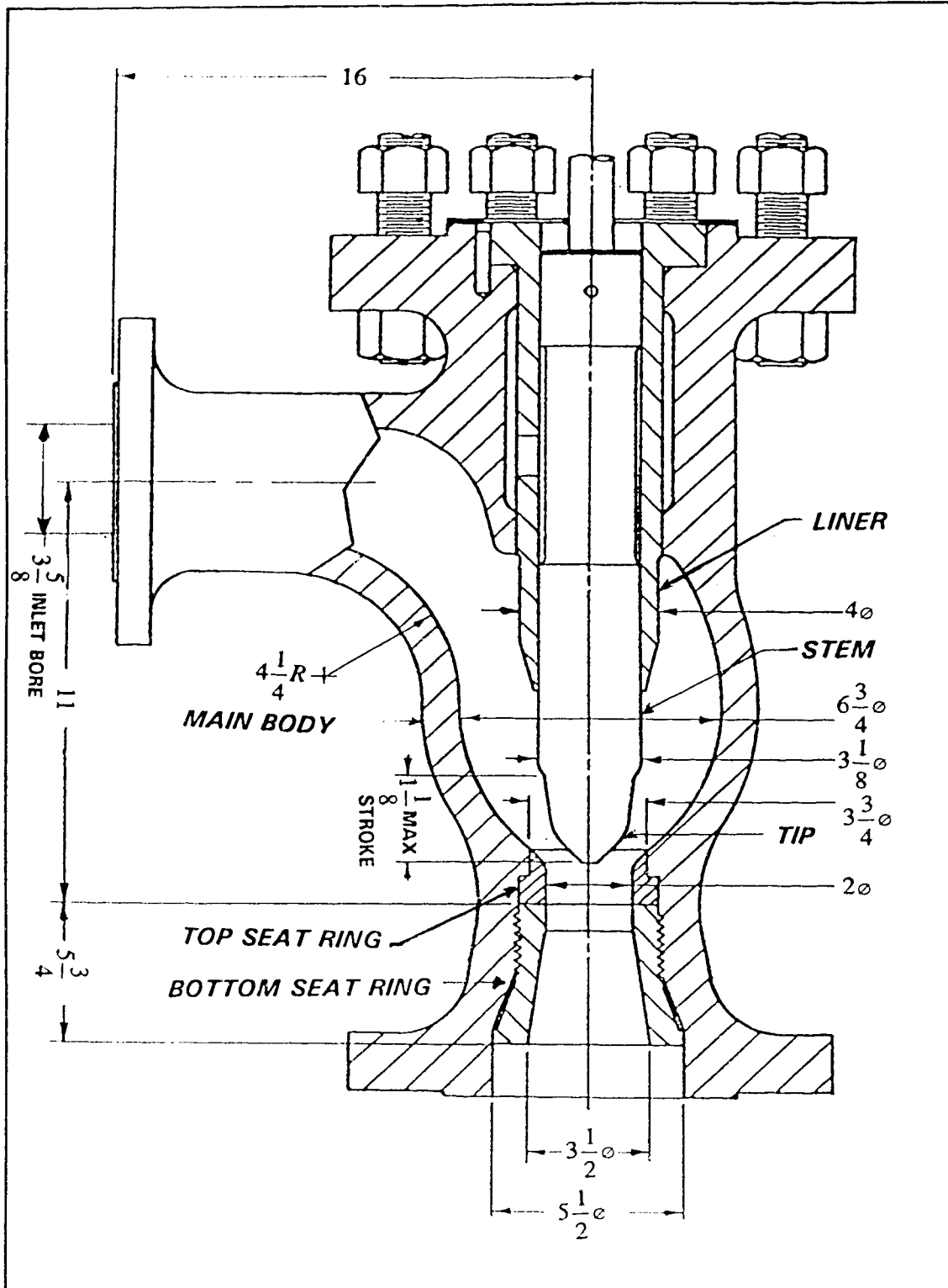


Figure 2.1. Valve cross section with labelled valve parts.

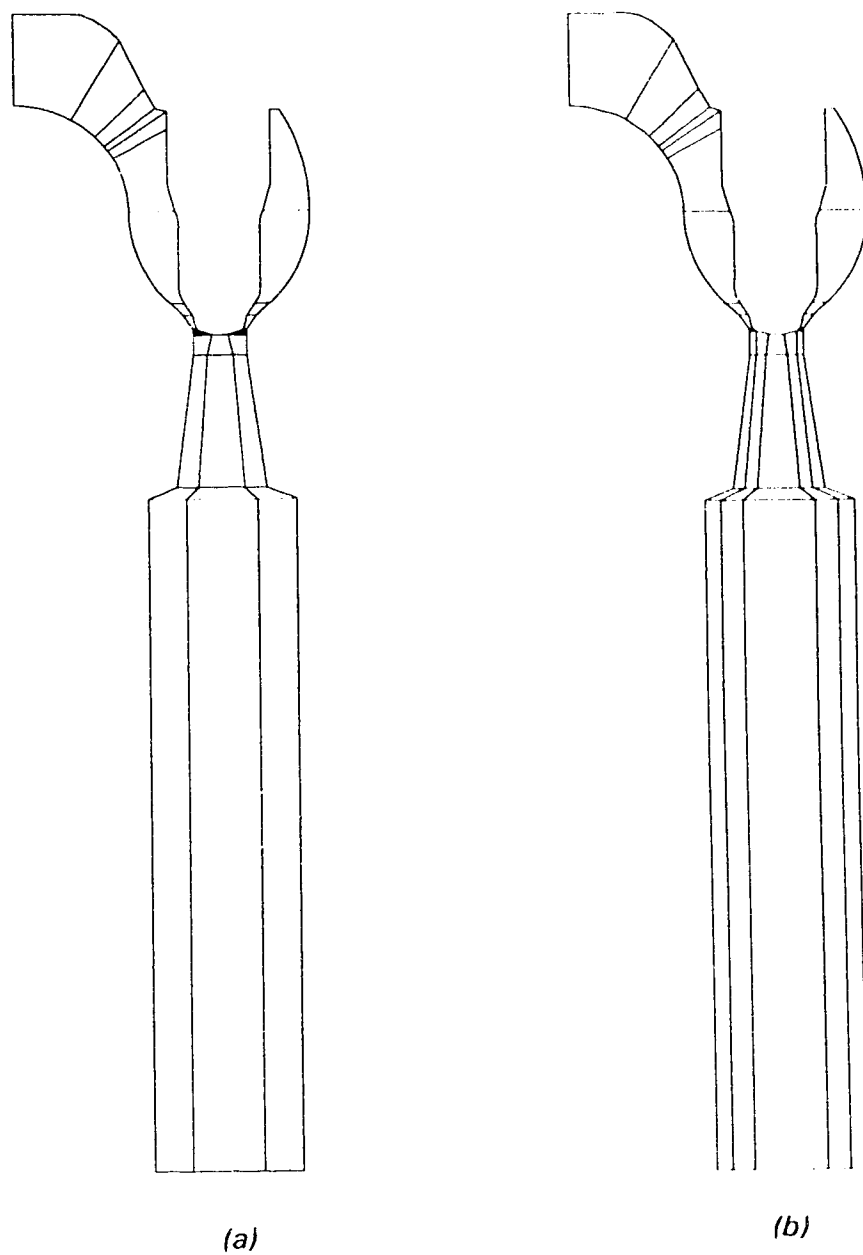


Figure 2.2. Cross section of multi-block structure. (a) 58 blocks, (b) 66 blocks.

Chapter 3

3.1 Governing Particle Properties in Solid Particle Erosion

The three fundamental particle properties that affect erosion are the mass of impinging particles, their impact velocity, and impact angle. Figure 3.1 shows the effect of impact angle on the erosion of ductile and brittle materials. The location of the maximum erosion rate is near impact angles of 20-30° for ductile compared to 90° for brittle materials. The erosion of most materials is proportional to the velocity raised to a power of 2-4 and is directly proportional to the mass of erodents. These three quantities (mass, velocity, impact angle) are dependent on the particle size, shape, and density. Particle density determines whether a particle will be highly inertial and impact valve surfaces where streamlines change direction. The Stokes Number which is defined as $S_t = \tau_p / \tau_f$ where $\tau_p = D_p d_p^2 / 18\mu$ and $\tau_f = L_c / U_c$, L_c and U_c are mean length and velocity scales. (Humphrey¹⁰) If the Stokes Number is $\ll 1$, the particle will tend to follow the flow streamlines, and if S_t is $\gg 1$, then particles are highly inertial and will not follow streamlines well, impacting valve surfaces. Thus, small particles will impact surfaces less frequently and at lower velocities than larger particles. For the present study the Stokes Number for the particles in the valve tip region varied from 1.1 to 113 for 10 and 100 μm particles respectively.

Smooth particles tend to cause significantly less damage compared to angular particles,

as shown by Levy et al¹⁴. Stropki^{12,13} found that the particles in the present application have smooth edges. Clearly for particles to cause significant damage to a surface, the particles must be at least as hard as the surface being eroded. The erosion dependence with hardness tends to be a step function with a very small increase in erosion with increases in particle hardness above the material hardness, as shown by Levy et al¹⁴. For this study the particles were assumed to have a hardness greater than the material being eroded.

Another aspect of particle impact is particle fragmentation, which affects the ability of particles to remain highly erosive. Stropki^{12,13} found that the ability of particles in the present study to cause erosion was constant with time, indicating negligible fragmentation.

Interference caused by rebounding particles on incident particles typically results in lower impact angles and possibly less impacts, as examined by Anand et al¹⁵ and Levy et al¹⁶. The rebounding particles reduce the normal component of velocity to the wall and thereby decrease the impact angles. Because we assume a dilute concentration, particle-particle interference is neglected.

3.2 Surface Effects of Solid Particle Erosion

The condition of the surface can have a major impact on erosion by establishing how

efficiently impacting particles will remove material. If the surface is highly grooved, scarred, and cracked, then impacting particles will have different impact velocities and angles as compared to those based on a smooth surface. With a highly scarred surface, the near wall velocity is substantially reduced relative to a smooth surface. Many researchers have noted the formation of regular erosion ripple patterns on surfaces which are also seen in the operational valve. (Karimi et al¹⁷), (Bitter^{18,19})

The evolution of the eroding surface typically is a time dependent function of the surface's initial condition and the erosion mechanism acting on it. The surface of the material plays a critical role in erosion, but in this simulation the surface was modelled as being smooth. This assumption is reasonable when the valve is new, but as the valve surfaces erode becoming rougher the accuracy will be reduced. Many of the edges in the valve between parts were modelled as perfectly smooth in order to simplify the already complex geometry. The operational valve has many edges from assembling the valve parts these are tool slots or holes, and grooves between individual parts such as the top seat ring to the main valve body.

3.3 Corrosion Effects on Erosion

Corrosion is a process controlled by molecular and turbulent diffusion and has been simulated by Nesic et al⁵ in a sudden pipe expansion. As indicated in section 3.2 the surface roughness will play a critical role in corrosion by establishing the turbulence

levels, as the turbulence levels increase so will corrosion.

Temperature has a significant effect on erosion-corrosion. Usually the wear rate increases with an increase in temperature to a maximum and then decreases. The reduction of wear after a critical temperature is due to the formation of more cohesive oxide layers. (Stacks et al²⁰) When selecting slightly different alloying materials in the present geometry, the wear rate was reduced slightly in the operational valve. This indicates that the operational valve may be operating in an erosion-corrosion state or the different alloying materials is simply more erosion resistant. Solid particle erosion is the dominate factor in wear of this valve as indicated by work from Stropki^{12,13}, and only the solid particle erosion was modelled in this simulation

With the formation of brittle oxide layers, the affect of impact angle on erosion can shift from ductile with most metal alloys to brittle fracture cracking of the brittle oxide layer. If a continuous and cohesive oxide scale can not be established, the corrosion-erosion rates will be very high.

3.4 Erosion Modelling of Steel Parts in the Valve

As mentioned in section 3.1 the erosion of ductile materials usually have maximum erosion rates at impact angles of 20-30°. At impact angles of less than 45°, the main erosion mechanism is a cutting wear process or mirco-machining (Finnie²¹). At angles

greater than 45° , the main mechanism of erosion is due to a fatigue or plastic deformation of the surface, as modelled by Hutchings²², Bitter^{18,19}, and Levy et al¹⁶ platelet mechanism.

For this simulation a modified Finnie's cutting wear model was used as suggested by Bergevin²³ and used by Nesic and Postlethwaite⁵ in their study. The modifications by Bergevin²³ includes Bitter's^{18,19} ideas for a critical velocity normal to the surface below which no erosion damage occurs since the impacting particle only causes elastic deformation. For the steel parts of the valve, the critical value was assumed to be 0.668 m/s as found by Bitter^{18,19}. Finnie's modified equations are as follows:

For $\theta \leq 18.5^\circ$

$$V \approx \frac{CM_p(U_p \sin \theta - U_{cr})}{2P} [U_p \cos \theta - 1.5(U_p \sin \theta - U_{cr})] \quad (3)$$

For $\theta \geq 18.5^\circ$

$$V \approx CM_p \frac{(U_p \sin \theta - U_{cr})^2}{12P} \frac{\cos^2 \theta}{\sin^2 \theta} \quad (4)$$

For angles of impact greater than 60° , Hutchings²² fatigue model was used to model the erosion. This is similar to suggestions by Majumdar et al²⁴ for combining Finnie's and Hutchings model in order to account for higher angle impacts. Stropki^{12,13} found

evidence of the importance of this fatigue mechanism in some operational parts of the valve and on 1018 CS test samples. The fatigue model was modified in a similar manner to Finnie's model with respect to a critical normal component of velocity to cause damage and is as follows:

For $\theta \geq 60^\circ$

$$V \approx k \sqrt{D_p} (U_p \sin \theta - U_{cr})^3 \quad (5)$$

There are numerous other erosion models but the determination of many constants makes their use difficult; these models can be attributed to Bitter^{18,19}, Neilson and Gilchrist²⁵, and Tabakoff et al². These models were not used due to the qualitative results of predicting the erosion prone areas was expected and the simplicity of Finnie's and Hutchings' models. The constants in the models for Finnie and Hutchings models were taken from work done by Majumdar et al²⁴, where a comparison of numerous experimental results and models is done.

A program was written which uses the results of the particle trajectories and calculates the resulting erosion. The erosion program determines the number of particles which impact a small area of the valve surfaces, and qualitative erosion rates are predicted using equations 3-5. Since the material constants P and K_f are not well known, the equations were non-dimensionalized by dividing by the maximum erosion rate (E_{max}).

This removed the material effect and produces qualitative results.

3.5 Erosion Modelling of WC-Co parts of the Valve

Tungsten carbide is commonly used as an insert in locations where severe erosion damage is occurring, such as slurry feed pumps and high pressure letdown valves (Wright et al²⁶) as in this study. The mechanisms involved in erosion of two-phase material such as this is very complex. Depending on the amount of brittle carbide (WC) and ductile Cobalt (Co) phase, the erosion can change significantly from the cutting of the ductile cobalt phase to the brittle fracture of the carbide phase.

A number of experiments by Conrad et al²⁷ indicate that if the crater from a single impact encompasses less than 10 WC grains, the mechanism is brittle. If it encompassed more than 100 WC grains, the erosion mechanism is ductile. For brittle material, the erosion is usually proportional to the normal component of velocity raised to an exponent, as first suggested by Hockey et al²⁸ and demonstrated by Conrad et al²⁹ for WC-Co.

The particles in the present study are in the size range of 10-20 μm as indicated by Stropki^{12,13}. For 30 μm particles Conrad et al²⁹ found that the maximum erosion occurred at an angle of impact of 90° with hard Al_2O_3 particles for WC-Co containing 4.5-11.3 wt % Co for the present valve, WC-Co containing 6-16 wt % Co are used indicating

erosion may be via a brittle mechanism. However tests by Stropki¹³ raise some concern that the erosion mechanism in the operational valve may be more ductile cutting of Co and sliding wear of WC grains. With Scanning Electron Microscope (SEM) the surface appeared polished, but the duration of the test was only 30 minutes and no measurable erosion occurred.

Several erosion models exist for brittle materials. We have chosen to use the Evan, Gulden, and Rosenblatt's³⁰ elastic-plastic model, one of three elastic plastic models which differ only in the power of their exponents. This model considers that impact particles cause the formation of two types of cracks, which are radial and lateral cracks, where the lateral cracks result in loss of material as shown by Evan et al³⁰. This model was modified by adding a critical velocity below which no damage occurs to the valve surface in a manner similar to the steel parts. The value of the critical velocity was assumed to be the same as steel 0.668 m/s since no experimental value was available. The model is as follows:

$$V \approx \frac{CD_m^{1/4} R_p^{11/3} (U_p \sin \theta - U_{cr})^{19/6}}{H^{1/4} K_c^{4/3}} \quad (6)$$

Conrad et al²⁹ found better correlation with this model at lower velocities and with smaller particles, which are similar to the velocities and particle sizes in this study.

With an experimental program an erosion model based on curve fits may provide more

quantitative results. In a study by Conrad et al³¹ a model is developed which accounts for the erosion of the ductile cobalt phase and brittle Carbide phase in WC-Co to predict erosion of WC-Co composite.

The two material parameters of Dynamic Hardness and Toughness are highly dependent on the erosion conditions. Values for the two constants were obtained from Conrad et al²⁹ since no experimental values were available. In addition the exponents for Dynamic Hardness and Toughness are uncertain as indicated by Laugier³². Therefore equation 6 was non-dimensionalized by dividing by E_{max} to allow for a qualitative indication of erosion locations and relative magnitudes.

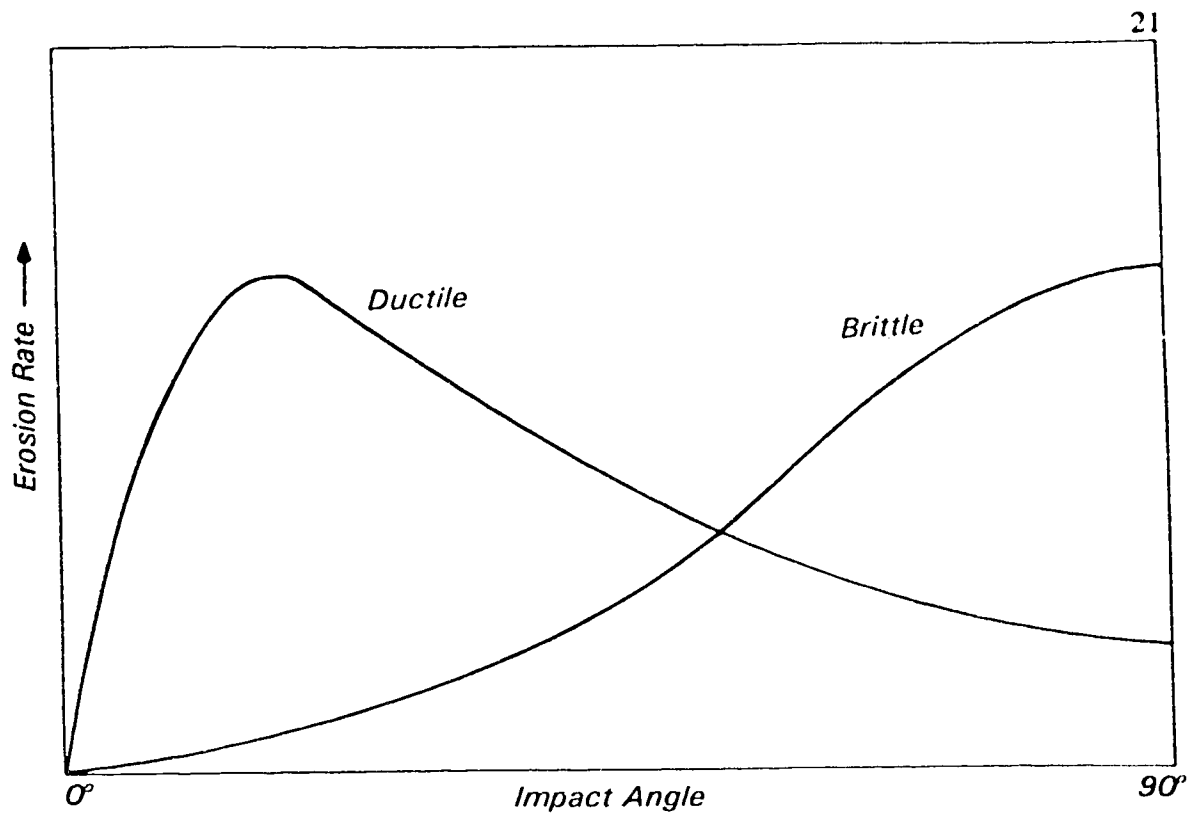


Figure 3.1. Schematic representation of erosion rate against impact angle.

Chapter 4

4.1 Flow Field

4.1.1 Grid Independence of the Flow Field

The complex geometry was gridded with a number of different density grids. The valve was divided into either 51,860; 95,856; 168,364; or 240,128 cells with 58 blocks as well as a substantially different block structure (66 blocks) with 135,000 cells. Two locations in the valve were chosen to compare grid independence; these two locations were the narrowest gap of the valve tip region and at the bottom of the lower seat ring. The non-dimensional parameters plotted at these locations is done in a similar manner to Prinos and Goulas³³ for flow characteristics downstream of a conical diffuser. As shown in figure 4.1 and figure 4.2 the non-dimensionalized profiles of U/U_m , k/U_m^2 and $\epsilon L_c/2U_m^3$ were similar to each other except for the very low density grid of 51,860 cells. The profiles of the turbulent dissipation rate ($\epsilon L_c/2U_m^3$) in the valve tip region were quite different for the three lower density grids as compared to the two highest density grids, especially near the seat ring wall. At the bottom of the lower seat ring the profiles of turbulent kinetic energy (k/U_m^2) and turbulent dissipation rate ($\epsilon L_c/2U_m^3$) are of the same shape, but the non-dimensional values have large variations. The modelled flow field should be reasonably accurate above the bottom of the valve tip (figure 4.1), since it is not affected by the recirculation zones below the valve tip as seen in the profile of U/U_m in figure 4.2. However, the presence of recirculation below the valve tip likely results

in poor performance of the $k-\epsilon$ model at the station shown in figure 4.2.

4.1.2 Analysis of the Flow Field in the Valve

Figure 4.3 shows the flow field for the 66 block structure with 135,000 cells for the main body of the valve above the seat rings. The velocity of the fluid in the upper section is less than 16 m/s. Near the bottom of the main body above the seat rings the velocity begins to drastically increase, reaching velocities of 36 m/s. There is only one small recirculation zone above the valve tip as shown in figure 4.3, and the pressure gradient is positive in this region indicating that the $k-\epsilon$ model should work well. The fluid is also a single phase hydrocarbon in this region of the valve.

The velocity in the tip region increases from 36 m/s at the top of the upper seat ring to 180 m/s at the valve seat as shown in figure 4.4. These high velocities clearly result in a highly abrasive situation when combined with entrained solid particles. The reattached jet of fluid to one side of the WC-Co insert also maintains velocities of 70 m/s throughout most of the length of the bottom seat ring. By the bottom of the lower seat ring the velocity has been reduced to approximately 20 m/s.

Below the valve tip the large regions of recirculation and the adverse pressure gradient raise concerns about the accuracy of the flow field. The $k-\epsilon$ model is known to perform poorly in areas of recirculation. With no experimental verification, the only indication

which may indicate that the jet of fluid will attach to one wall is the erosion of the WC-Co inserts predominantly on one side in the operational valve. Flow visualization of diffusers commonly exhibits this type of instability, indicating that this is a realistic flow pattern.

The model's agreement with the pressure drop across the valve was poor. The operational valve's pressure drop is 8067 kpa whereas FLOW3D predicts a drop of 5000 kpa as shown in figure 4.4. The large difference in the pressure drop may be attributed to inaccuracies of the $k-\epsilon$ model in an adverse pressure gradient. In addition, the fluid phase is a multi-phase hydrocarbon stream which would flash and expand at the lower pressure in the valve seat and tip region. This would result in an increased velocity in the valve seat region and therefore increased pressure drop, when compared to this single phase fluid simulation. The simulated pressure drop in the valve seat was 11,000 kpa which is as high as the upstream pressure of 11,000 kpa. On some wall nodes in the valve seat region even lower pressures were predicted; this low pressure and the type of operating conditions indicate the potential for cavitation to occur.

The calculated flow coefficients (C_v) through the valve were in better agreement with manufactures C_v for single phase fluid as shown in figure 4.5. The difference is approximately 20 percent.

4.2 Particle Trajectories Through the Valve

4.2.1 Particle Impact Results

The trajectories of 10, 20, 50, and 100 μm particles through the valve are shown in figure 4.6. The figure shows a projection of the particle trajectory on a cross section of the valve. The trajectories of the particles are similar except for the location where the 50 and 100 μm particles impact the valve tip. Centrifugal forces tend to force the 50 and 100 μm particles farther out towards the bend due to their greater mass.

Particle impact results are plotted in figures 4.7-4.14. The mass flux of impacting erodents increases with particle size as expected due to increasing Stokes number. The greatest number of impacts occur in the valve seat and tip region as shown in figures 4.9 & 4.11 which are projections of the particle impact results of the interior valve surfaces on to a valve cross section. The particle flux on the surfaces of the seat rings is much higher than the valve tip; this is due to the sharp edge of the valve seat in the upper seat ring and the smoothness of the gridded valve tip. The maximum mass flux varies from 3.3 ($\text{g}/\text{cm}^2\text{s}$) for the 10 μm particles to 15 ($\text{g}/\text{cm}^2\text{s}$) for 100 μm particles on the interior surfaces of the valve. The impacting particle flux above the valve seat rings is low for all sizes of particles, and below the valve tip it is only a small fraction of the value in the valve seat region. The maximum flux of particles on the valve plug surfaces varies from 0.8 ($\text{g}/\text{cm}^2\text{s}$) for 10 μm particles to 3.0 ($\text{g}/\text{cm}^2\text{s}$) for 100 μm particles. The flux of

impacting particles is not uniformly distributed on a cross section, as seen in figures 4.10 & 4.12 for the 20 and 50 μm particles. Note the locations on the wall which are subject to substantially higher than the average particle mass flux. This can be attributed to not tracking enough particles or locations in the operational valve where preferential erosion is taking place.

The impact velocity increases greatly with particle size as indicated in figures 4.7-4.14. This relationship can be directly attributed to the particle Stokes numbers. Particles which were 10 μm in size have impact velocities of 35 m/s in the valve seat, 10 m/s at the bottom of the lower seat ring, and less than 4 m/s in the remainder of the valve, these velocities are insufficient to cause material loss. For the larger 100 μm particles the velocity in the valve seat region was approximately 50 m/s. As with the flow field, the impact velocity of the particles increases as the valve seat is approached and then decreases after the valve tip.

The impact velocities on the surfaces of the valve plug assembly were systemically lower than for the valve seat ring surfaces. This can be attributed to the removal of sharp edges on the valve plug as compared to the sharp edge of the upper seat ring at the valve seat as shown in figure 2.2. The particle impact velocity for the valve plug varied between 18 and 40 m/s for the 10 and 100 μm particles respectively. These velocities are high enough to cause significant wear. Figures 4.10 and 4.12 show local high impact velocity locations for 20 and 50 μm particles.

As described in section 2.1, the type of erosion mechanism is determined by the impact angle and therefore impact angle plays a key role in material selection for erosion resistance. In the valve seat and tip region the majority of impact angles are less than 25°. The streamlined shapes of the valve tip and seat rings causes these low impact angles. WC-Co is brittle and suffers maximum erosion at impact angles of 90° as discussed in section 3.5. This low impact angle therefore explains the excellent performance of WC-Co inserts in this region.

In the bottom seat ring, impact angle tends to be much higher with a value of approximately 40° increasing the erosion rate of this section. The impact velocities are lower except for the localized high impact velocities which may result in the formation of regular ripples in the eroded surface seen in the operational valve. The simulated impact angles for the 10 μm particles are slightly higher due to an increase in the effect of turbulent dispersion.

The main body above the seat rings and the top section of the upper seat ring have impact angles of approximately 30°, at which maximum erosion occurs for the steel material of these parts. By altering the contours in the valve seat and tip region the particle trajectories could be altered to reduce the impact angles, and thereby, reduce the erosion rate.

4.2.2 Effect of Turbulent Dispersion

Figure 4.15 shows the trajectories of a 10 μm particle with and without turbulent dispersion. The turbulent dispersion particle trajectory is relatively smooth above the valve tip but irregular below the tip in comparison to the non-turbulent dispersion particle trajectory. With turbulent dispersion the number of impacts observed was substantially higher, with a tendency for the impact angles to increase slightly. The random fluctuations of turbulent dispersion also provide an additional force on particles moving parallel to the wall to impact and eject slow moving particles from the boundary layer. Without turbulent dispersion this simulation predicted almost no erosion except for narrow bands at the valve tip.

4.2.3 FLOW3D Particle Tracking Problems

When tracking particles with FLOW3D a large percentage of particles appear to become trapped in boundary layers due to their slow speed, and are not tracked further in the valve. This results in inaccuracies in the erosion modelling. Increasing the time limit to track an individual particle through the valve has almost no effect if a particle's velocity is nearly zero, and it substantially increases computational time. Fixing this problem is necessary to increase model accuracy and dependability. Benim et al³ developed particle tracking routines to replace FLOW3D's particle tracking routines for the simulation of erosion in a turbocharger radial turbine.

4.3 Comparison of Simulated to Operational Wear Patterns

The initial reason for simulating the erosion in this control valve was to determine the feasibility of such a simulation. If feasible, then such simulations could be used as an additional tool for evaluating methods to reduce erosion of the valve. Without additional experimental data, comparison of the operational wear patterns to the simulation wear patterns is the only method available to verify qualitatively the flow field and particle trajectories.

Figures 4.16-4.18 show the results of the simulation in comparison to the operational valve. In order to identify locations with varying erosion, the non-dimensionalized erosion from section 3.4 & 3.5 was scaled from 0 to 5 with 5 being severe erosion, this is similar to work by Ahmad et al⁴ to classify erosion. Eroded valve parts and discussions with Syncrude personnel were used to classify the erosion of the operational valve on this scale of 0 to 5.

The erosion of the upper main body above the seat rings in both the simulation and the operational valve occurs just above the upper seat ring as shown in figure 4.16. The erosion is not severe for 10 and 20 μm particles as indicated by the qualitative erosion rate of 0.2 on a scale of 0-5. The erosion rate of 0.9 for 50 and 100 μm particles is over four times higher in this region. The operational valve experiences a greater amount of erosion with a relative value of 1.2, as shown in figure 4.16. The difference between

the simulation and the operational valve is caused by a rough transition from the main valve body to the seat rings. The transition disrupts the flow causing increased turbulence and therefore causes increased erosion.

The simulation predicted some wear at the top of the inlet bend but the operational valve did not experience any erosion in this location. The simulated valve had low erosion here for all sizes of particles studied.

In the valve seat region, the top seat ring experiences erosion of the metal part and the WC-Co insert, which agrees with the simulation. The erosion of the seat rings in the valve is very severe as indicated by the large area of the seat rings with erosion values greater than 3 in figure 4.17. The erosion tends to be localized to one side in the operational valve as shown in figures 4.17 & 4.19. The simulation also shows locations of preferential erosion due largely to the flow patterns of the fluid jet attaching to one side figure 4.4.

The high erosion rates of the seat rings can be directly attributed to the high velocity of the impacting particles and the large mass of impacting particles. The large 50 and 100 μm particles overestimated the erosion of the WC-Co inserts, while comparison was better with the 10 and 20 μm particles. The operational valve contained large ripple structures that qualitatively agree with the simulation results, due to the local high erosion locations as shown in figure 4.17.

The simulation underestimated the severity of erosion in the valve stem and tip as shown in figure 4.18. The operational valve experiences much higher erosion than the simulation in the tip region; a high erosion rate is occurring as indicated by the operational wear rate of 5 compared to the simulation rate of 3.6-4.0. In addition, the valve stem of the operational valve suffers a small amount of erosion but no erosion was modelled in the simulation. This is due to simulating this region using a smooth rather than abrupt transition, see figures 2.1 and 2.2.

The simulated wear patterns of the valve tip had localized regions with high values of erosion as shown in figure 4.18. This agrees with the erosion of the operational valve tip to one side as shown in figures 4.18 & 4.20.

Even though the simulation tended to underpredict the level of erosion, the simulation still provides a good model of relative erosion rates between regions. The principle reasons for the lower values are likely caused by the simulated shape being more streamlined in the simulation than the actual valve tip assembly, and not tracking enough particles.

The simulation was able to demonstrate that the most likely sizes of particles 10-20 μm particles (Stropki^{12,13}) are causing the erosion of the valve.

As the valve is operated the erosion of preferential locations should worsen with time as

the flow takes the path of least resistance, and the surfaces become rougher. Erosion predominantly to one side would cause the flow to attach to that one wall even more by increasing the diffuser angle in the lower seat ring, as indicated by the wear patterns of the operational valve.

Quantitative results are not possible with such a large number of uncertainties in the flow field, particle tracking, erosion models, and material constants. Overall the qualitative agreement with the operational valve appears reasonable considering the large number of assumptions.

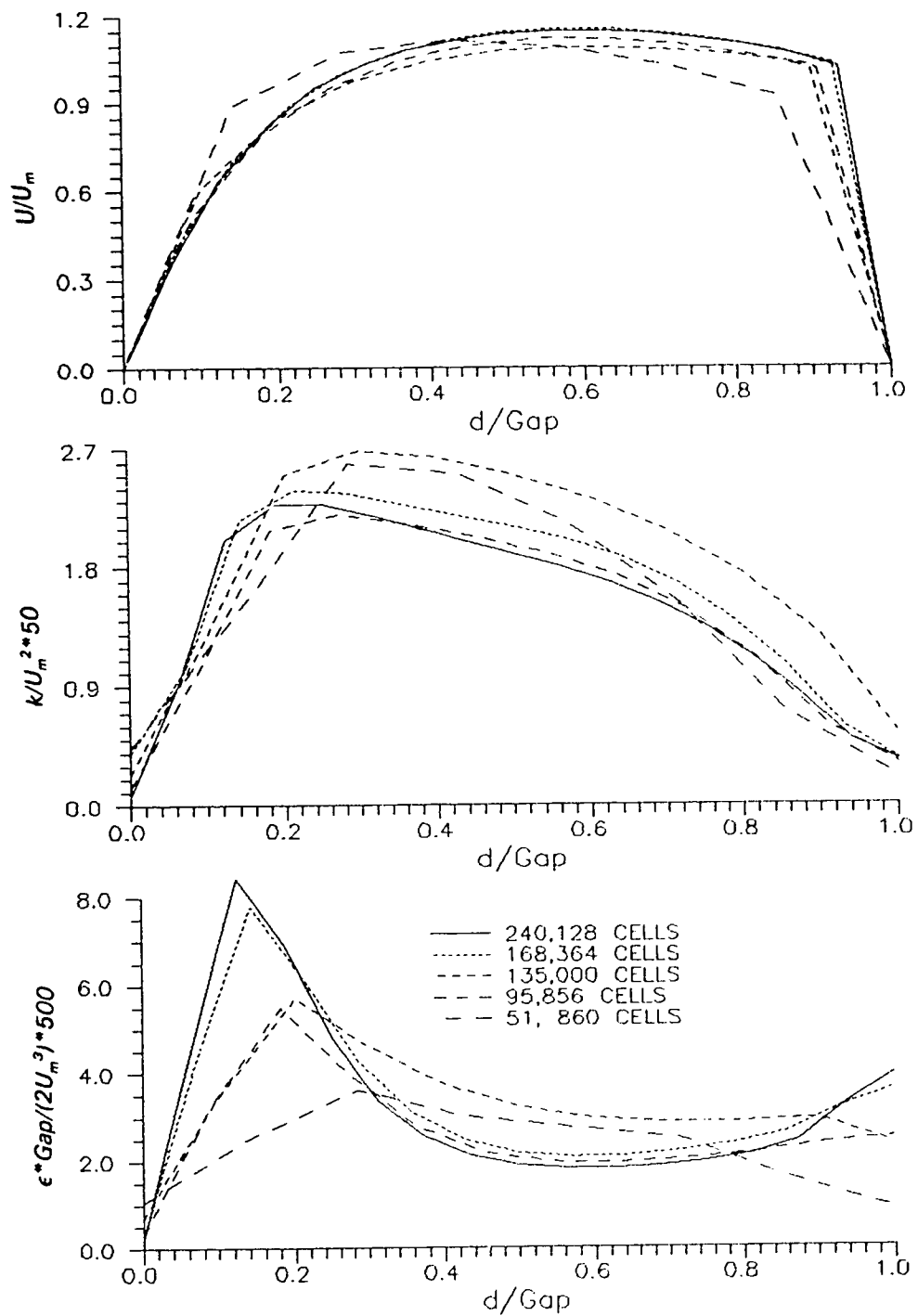


Figure 4.1. Effect of grid refinement on flow characteristics in the valve tip region. [Gap 6.18mm, outside wall is at $d/\text{Gap} = 0.0$, tip wall is at $d/\text{Gap} = 1.0$.]

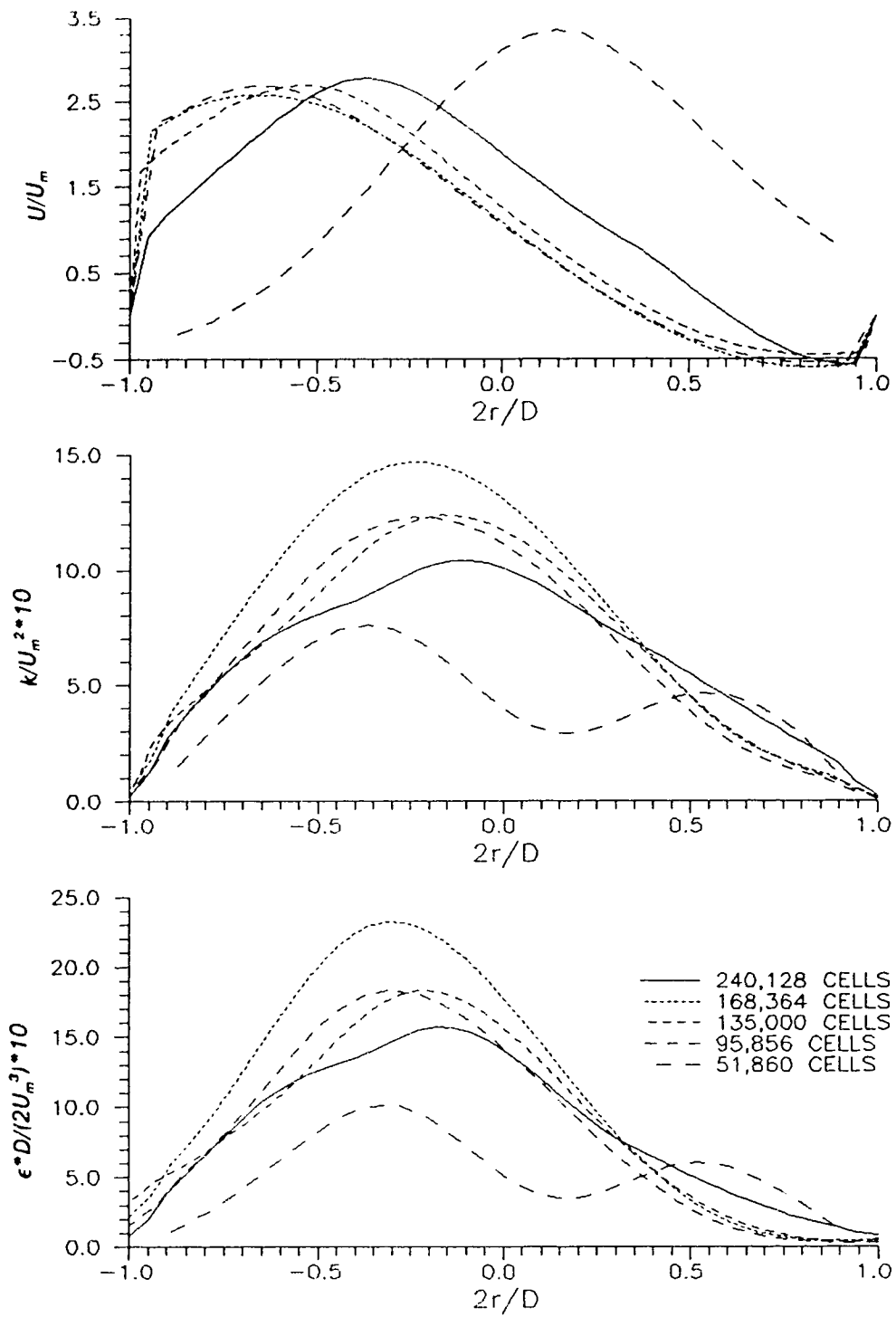


Figure 4.2. Effect of grid refinement on flow characteristics at the bottom of the valve seat rings. [r 42.86 mm, D 85.72 mm.]

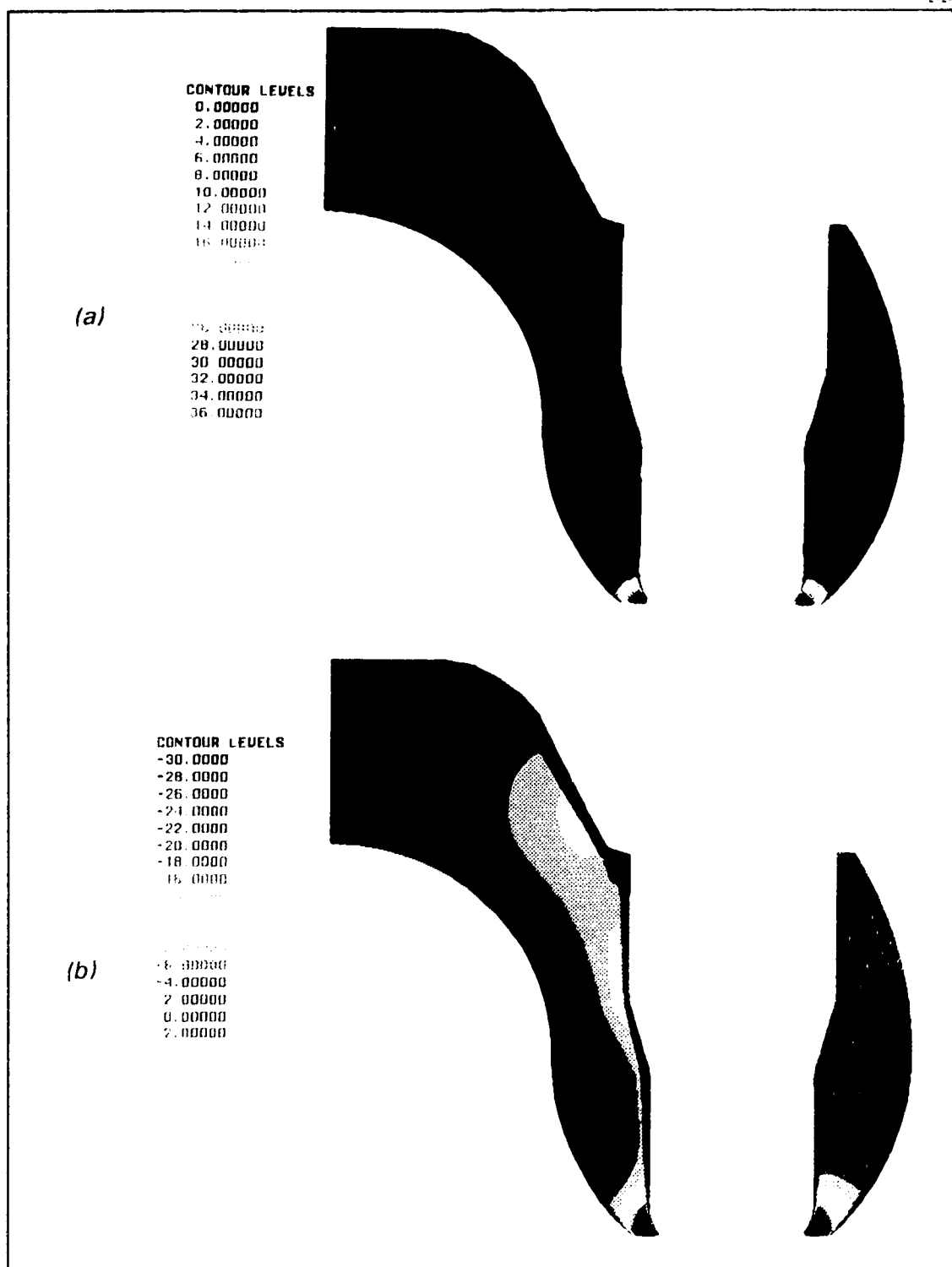


Figure 4.3. Cross section of flow field in main body of valve. (a) Velocity Magnitude (m/s), (b) Vertical Velocity (m/s).

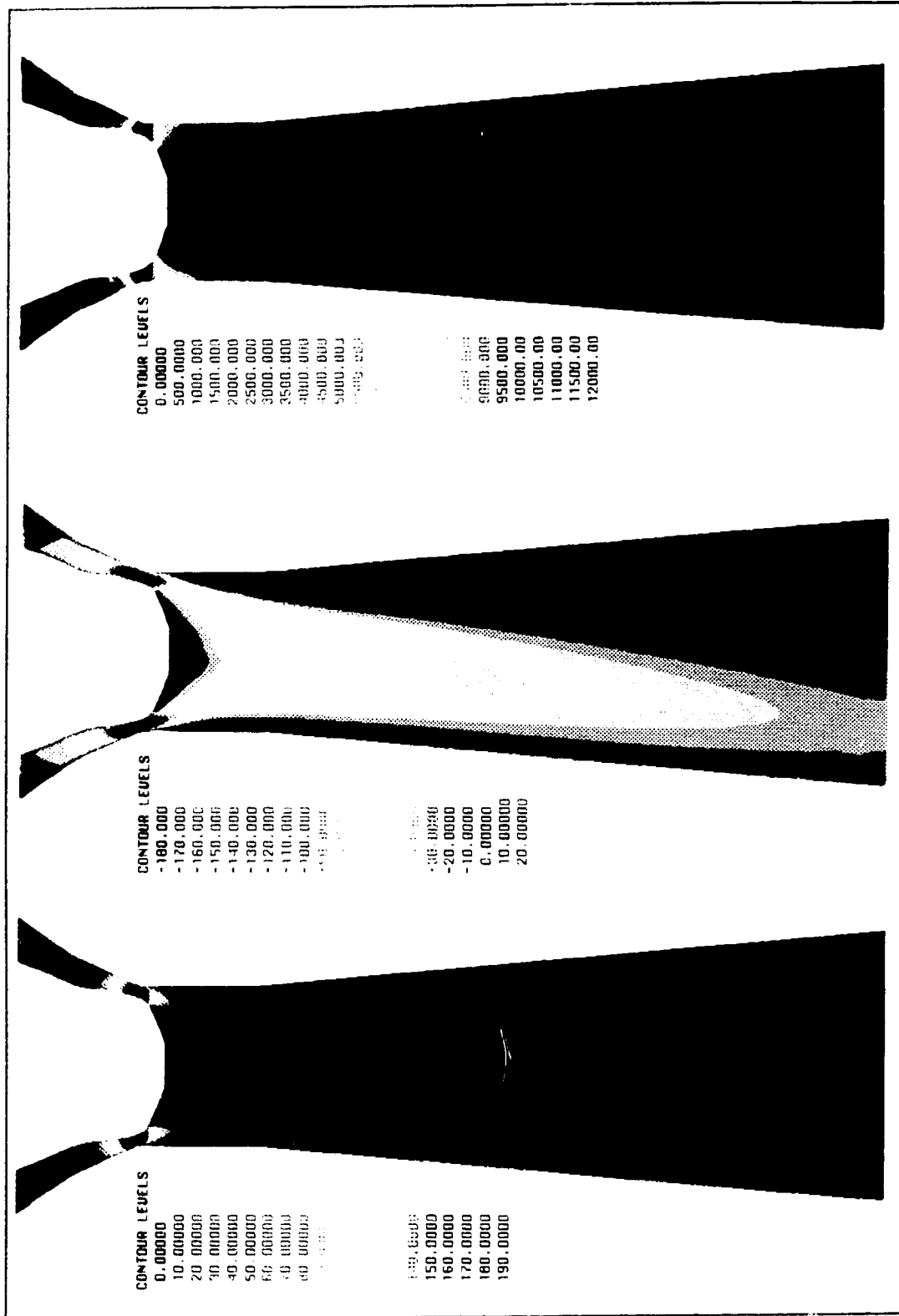


Figure 4.4. Cross section of flow field in valve seat rings. (a) Velocity magnitude (m/s) (b) Vertical velocity (m/s), (c) Pressure drop (kpa).

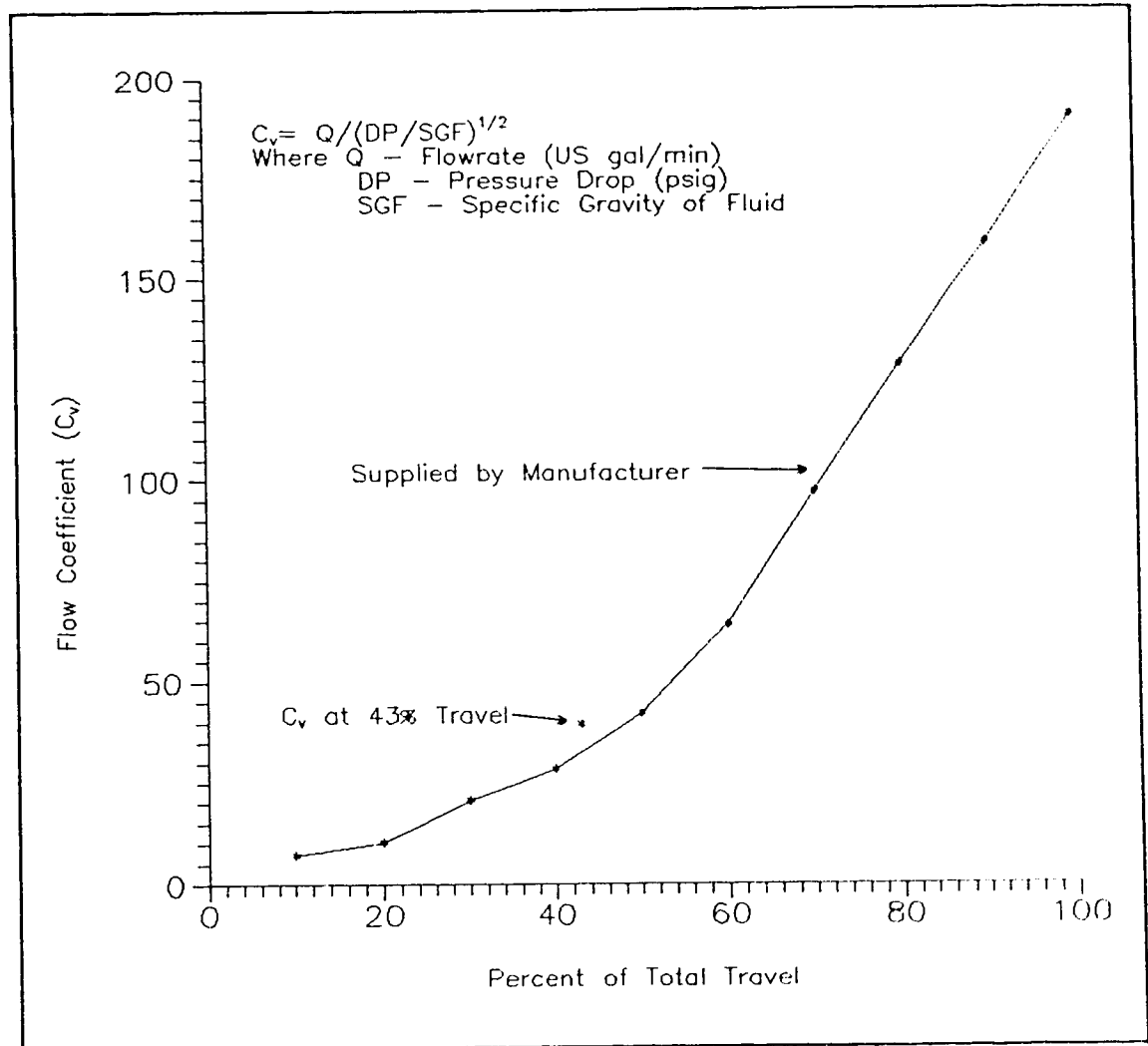


Figure 4.5. A comparison of measured flow coefficients to the simulated flow coefficient with the percentage of valve travel.

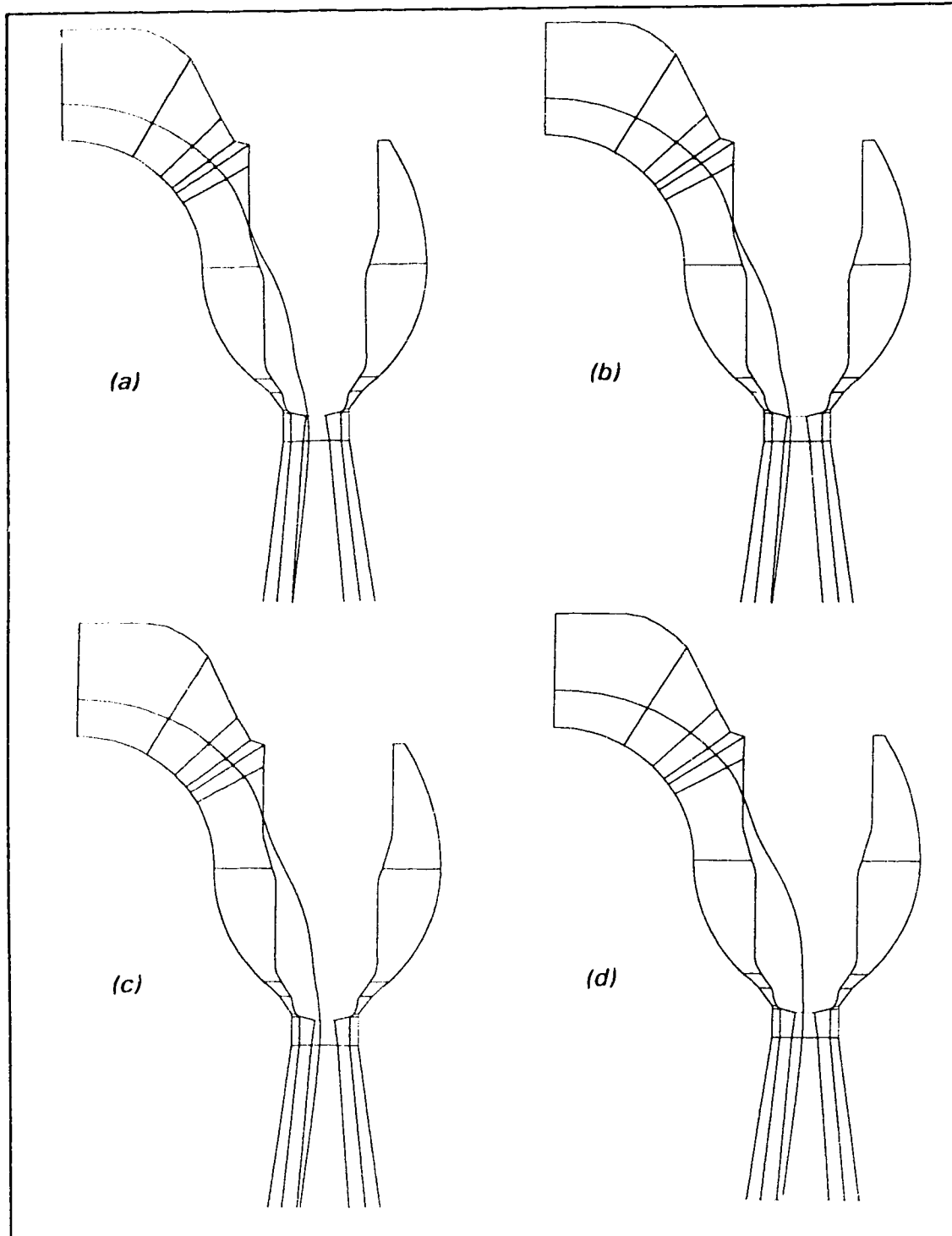


Figure 4.6. Comparison of particle trajectory with particle size. (a) 10 μm , (b) 20 μm , (c) 50 μm , (d) 100 μm .

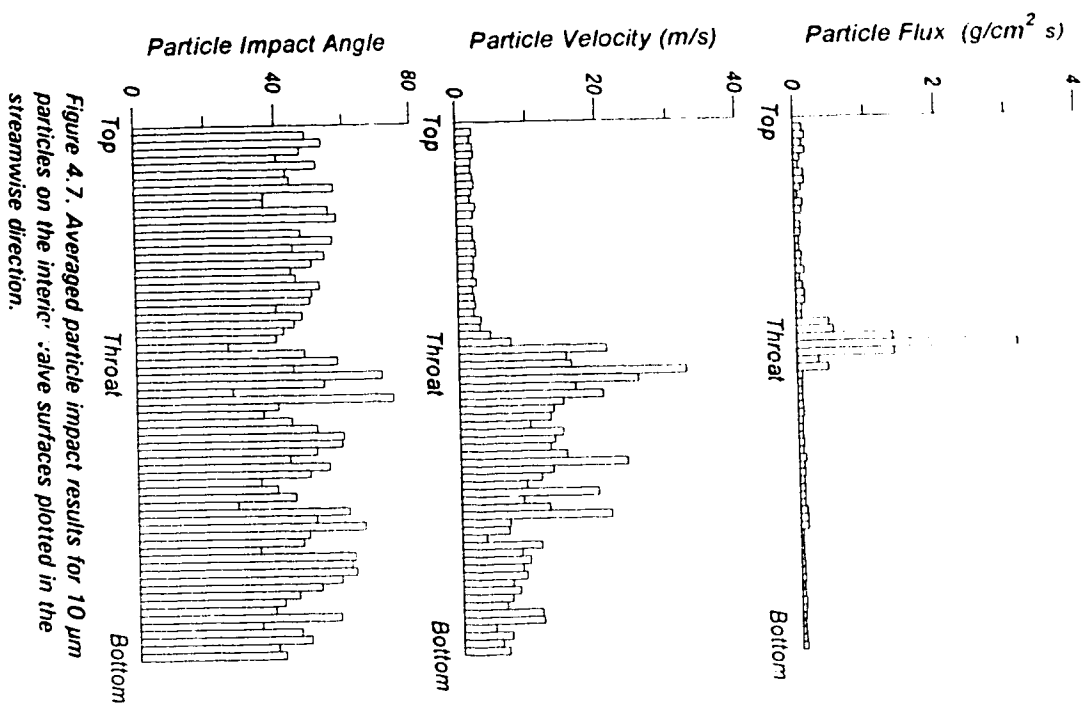


Figure 4.7. Averaged particle impact results for 10 μm particles on the 'interic' valve surfaces plotted in the streamwise direction.

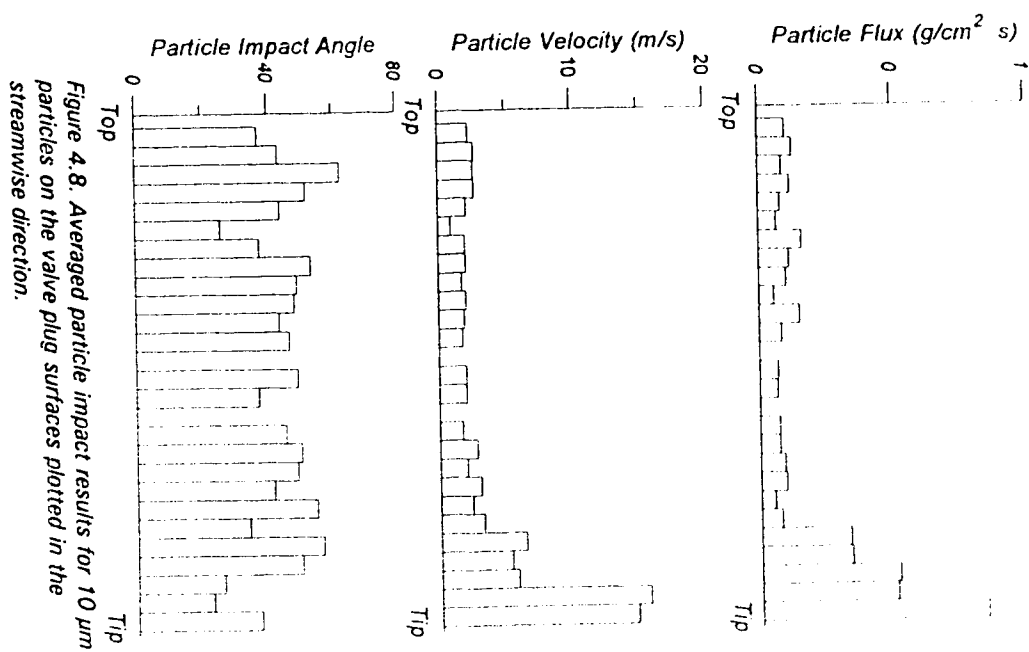


Figure 4.8. Averaged particle impact results for 10 μm particles on the valve plug surfaces plotted in the streamwise direction.

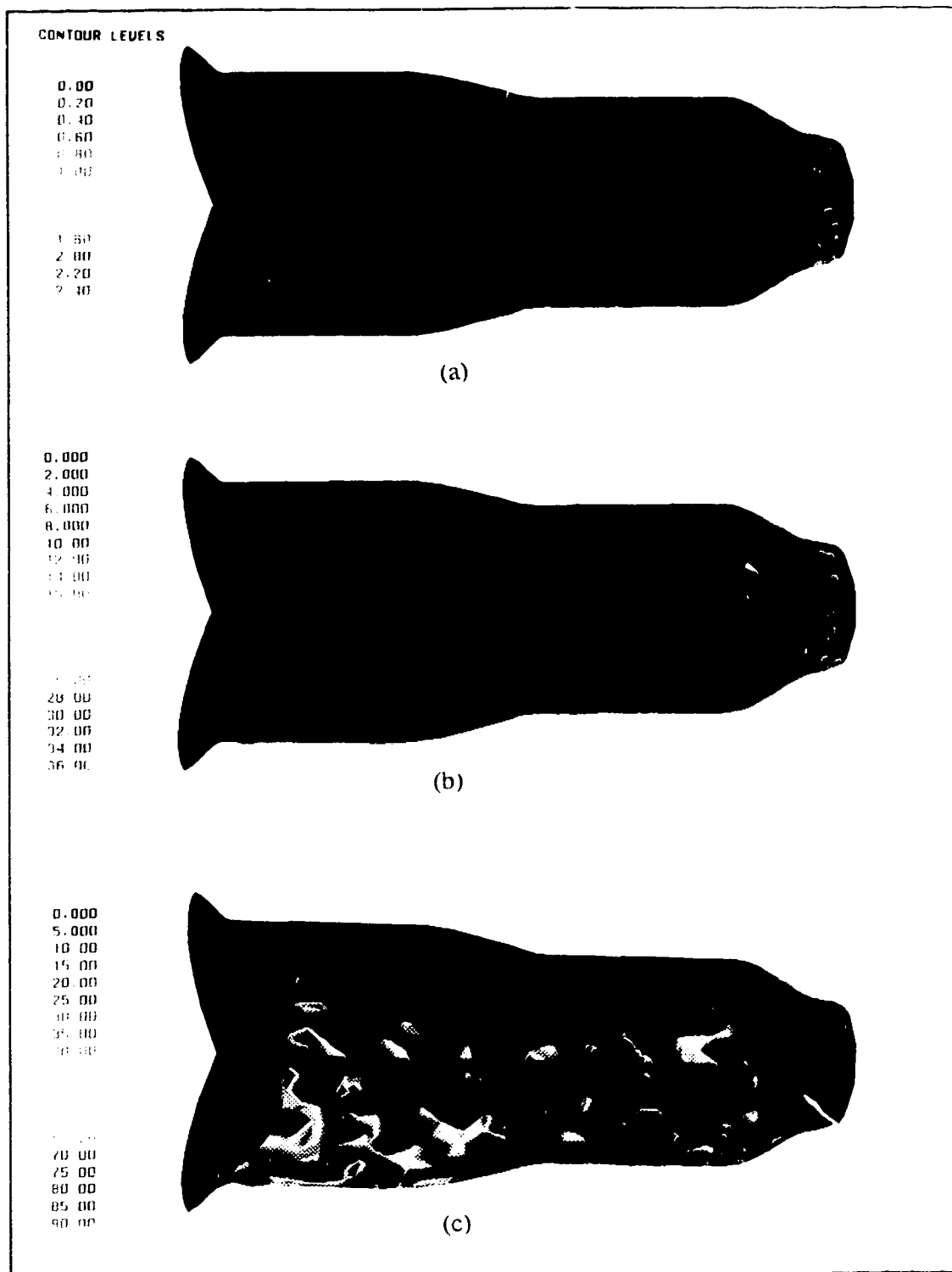


Figure 4.10. Particle impact results for 20 μm particles on the valve plug surfaces. (a) Flux ($\text{g}/\text{cm}^2\text{s}$), (b) Velocity (m/s), (c) Impact Angle.

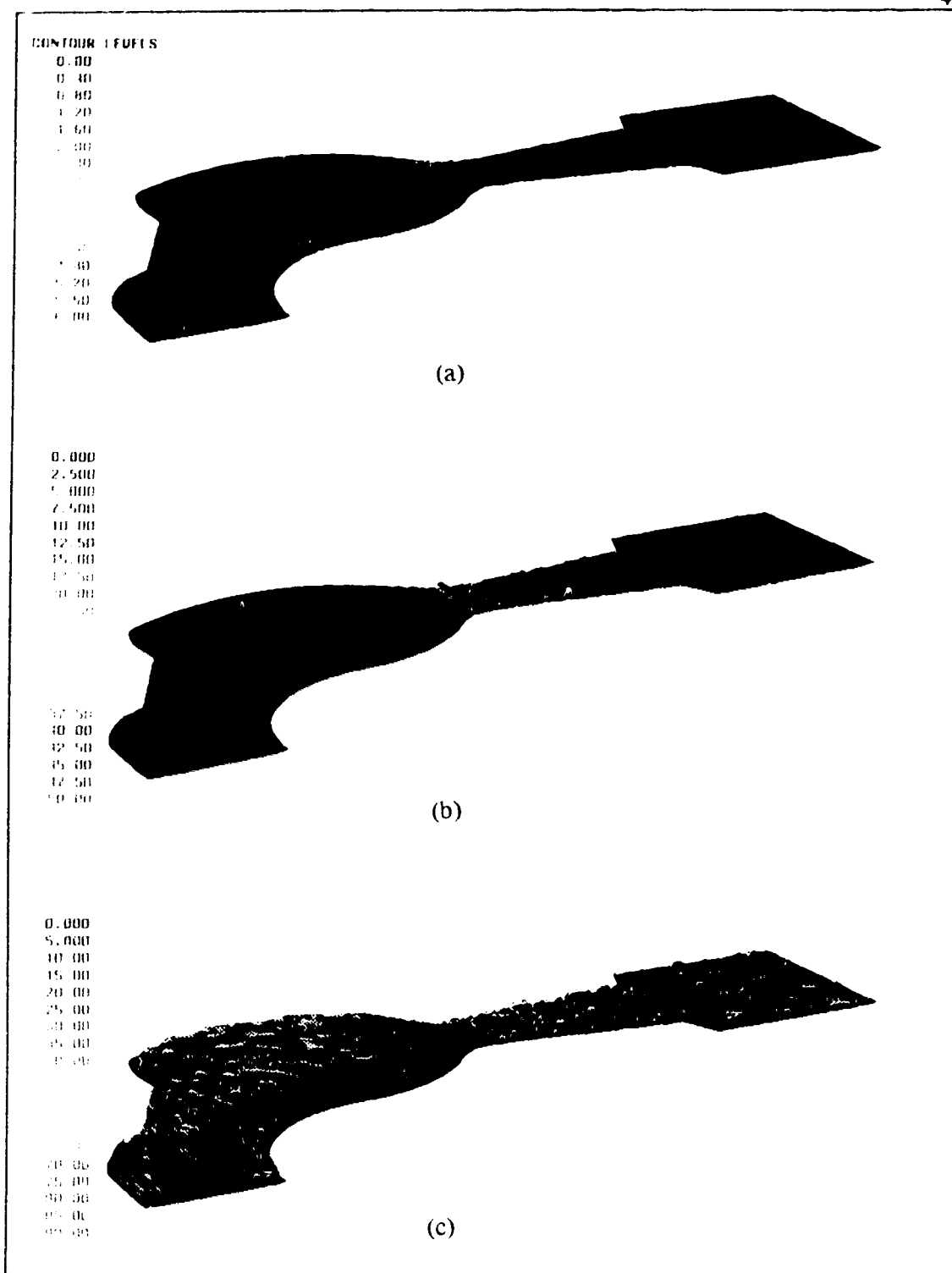


Figure 4.11. Particle impact results for 50 μm particles on the interior valve surfaces. (a) Flux ($\text{g}/\text{cm}^2\text{s}$), (b) Velocity (m/s), (c) Impact Angle.

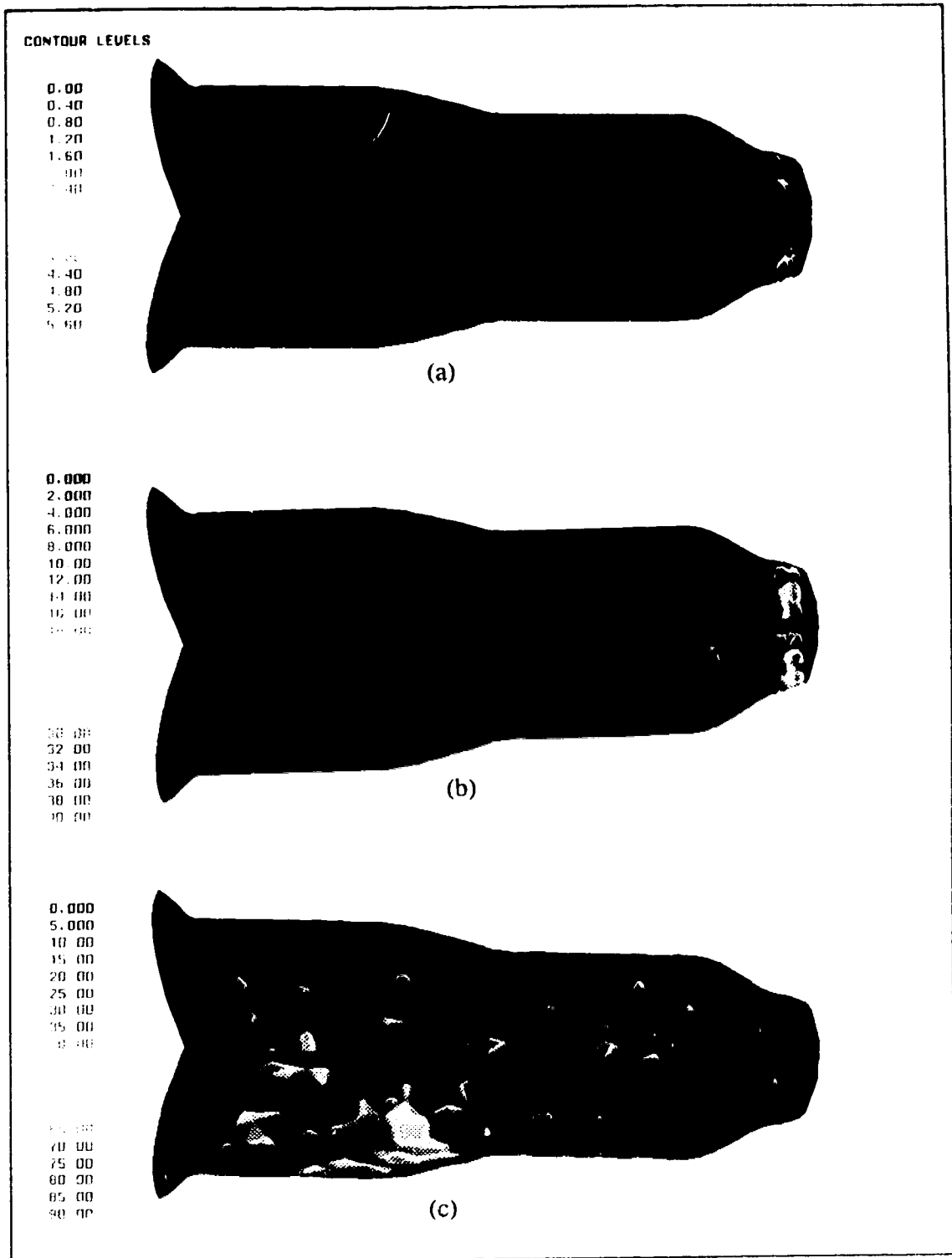


Figure 4.12. Particle impact results for 50 μm particles on the valve plug surfaces. (a) Flux ($\text{g}/\text{cm}^2\text{s}$), (b) Velocity (m/s), (c) Impact Angle.

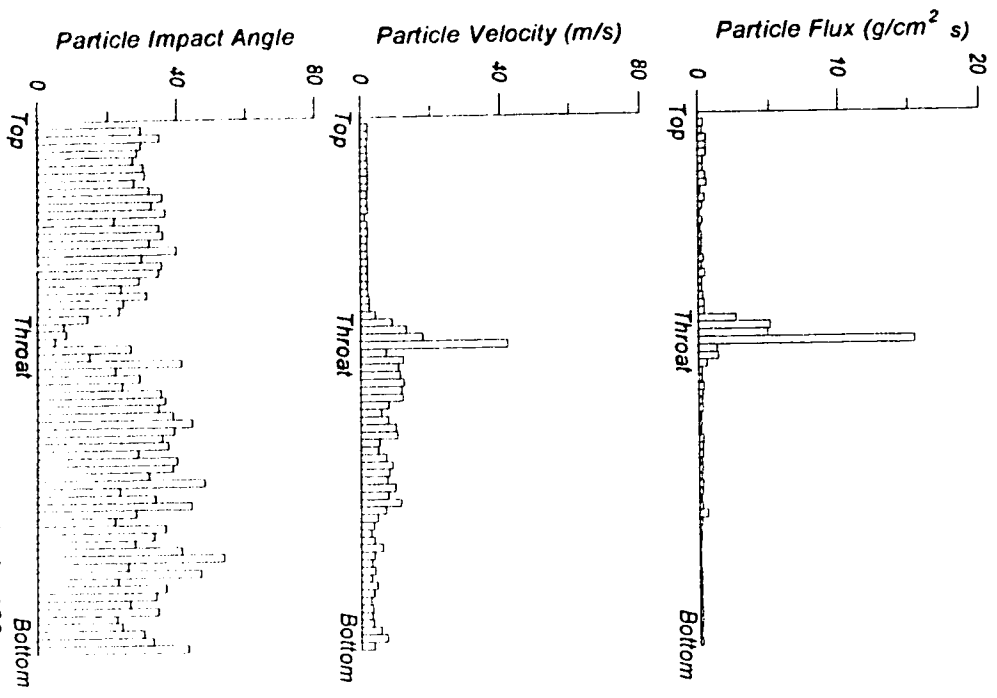


Figure 4.13: Averaged particle impact results for 100 μm particles on the interior valve surfaces plotted in the streamwise direction.

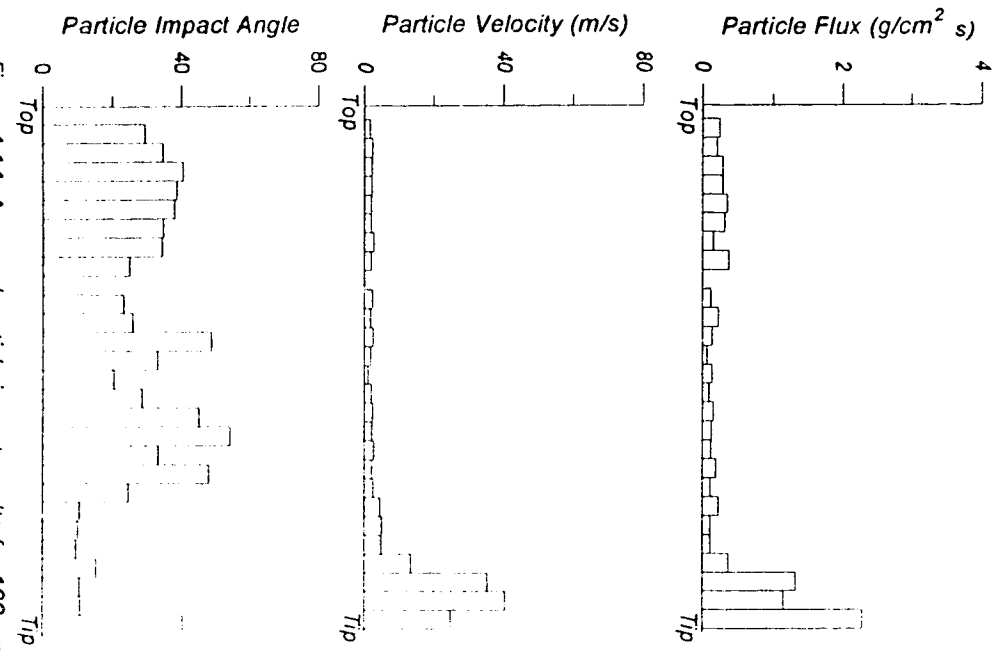


Figure 4.14: Averaged particle impact results for 100 μm particles on the valve plug surfaces plotted in the streamwise direction.

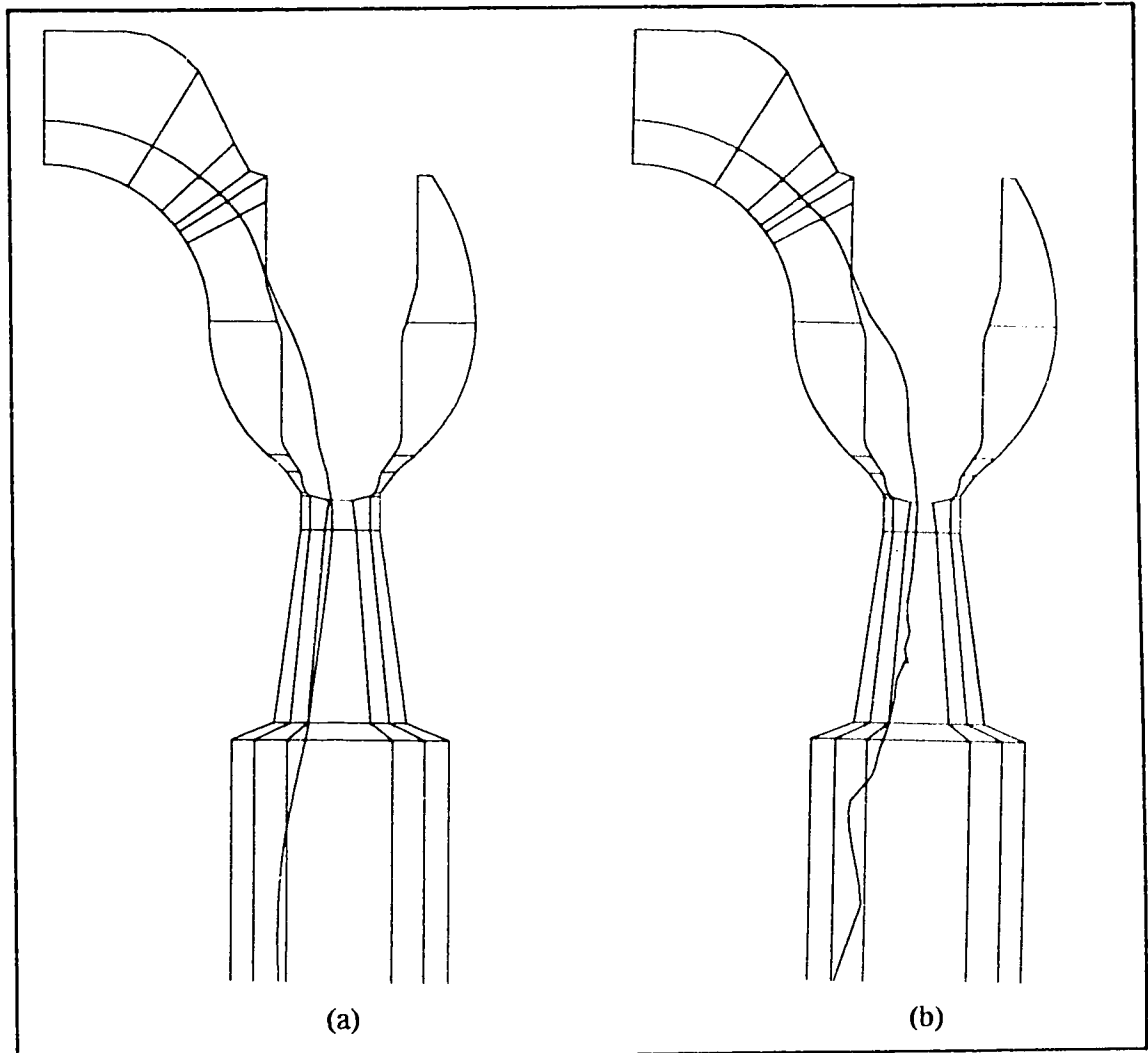


Figure 4.15. Particle trajectories with and without turbulent dispersion for 10 μm particles. (a) Neglected, (b) Included.

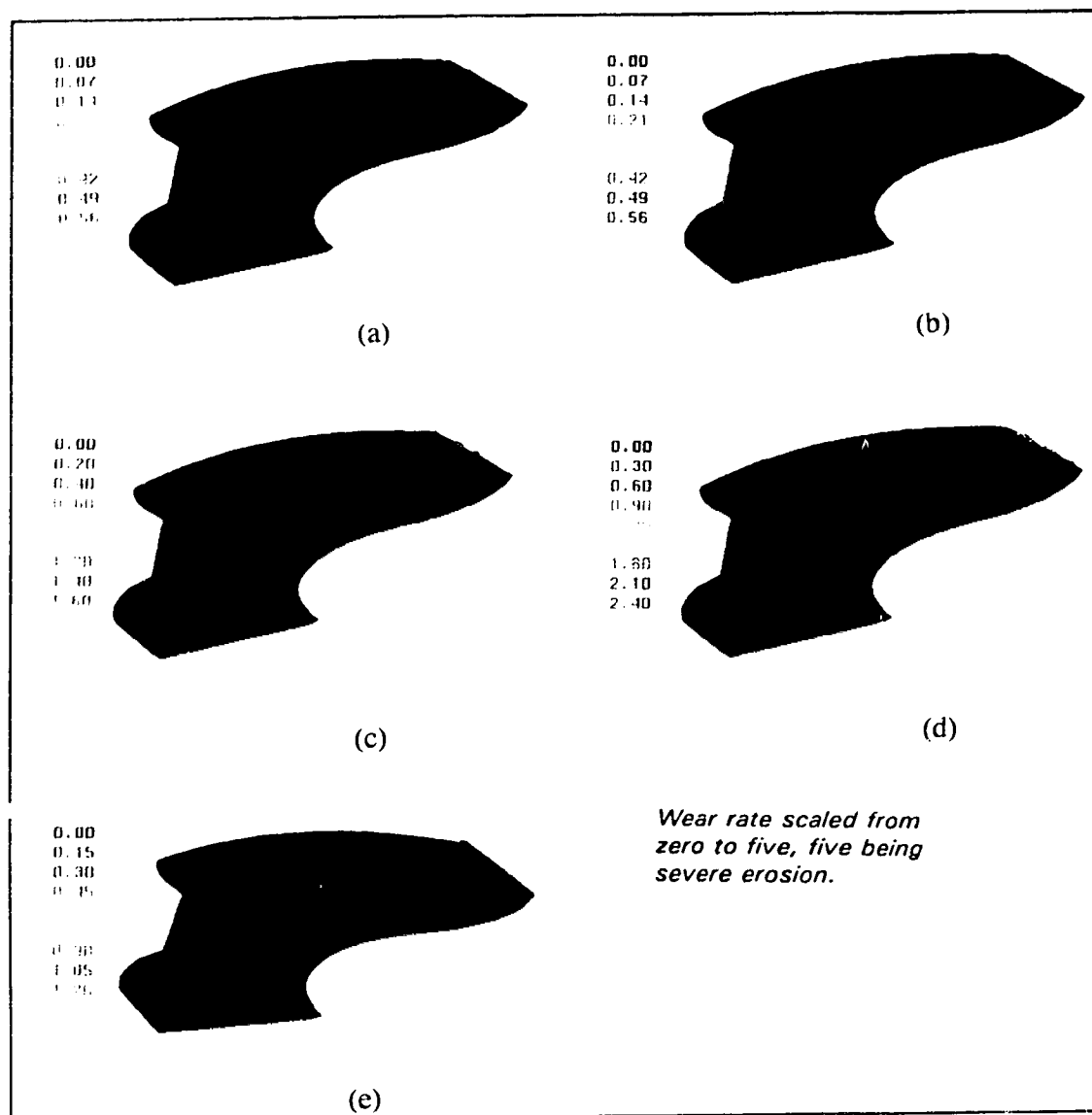


Figure 4.16. Comparison between predicted and actual wear patterns for the valve's main body. (a) 10 μm , (b) 20 μm , (c) 50 μm , (d) 100 μm , (e) Operational valve.

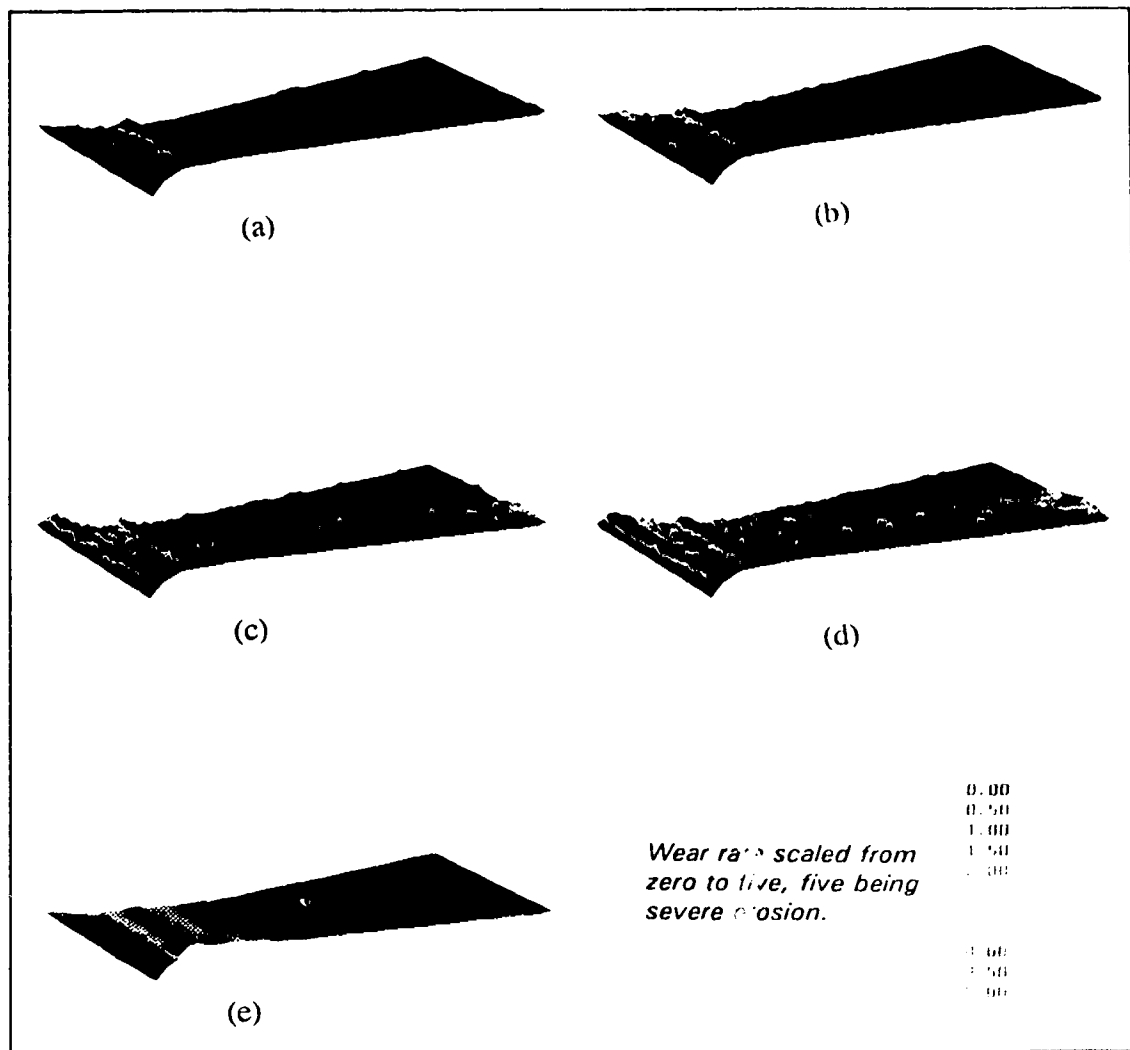


Figure 4.17. Comparison between predicted and actual wear patterns for the valve seat rings. (a) 10 μm , (b) 20 μm , (c) 50 μm , (d) 100 μm , (e) Operational valve.

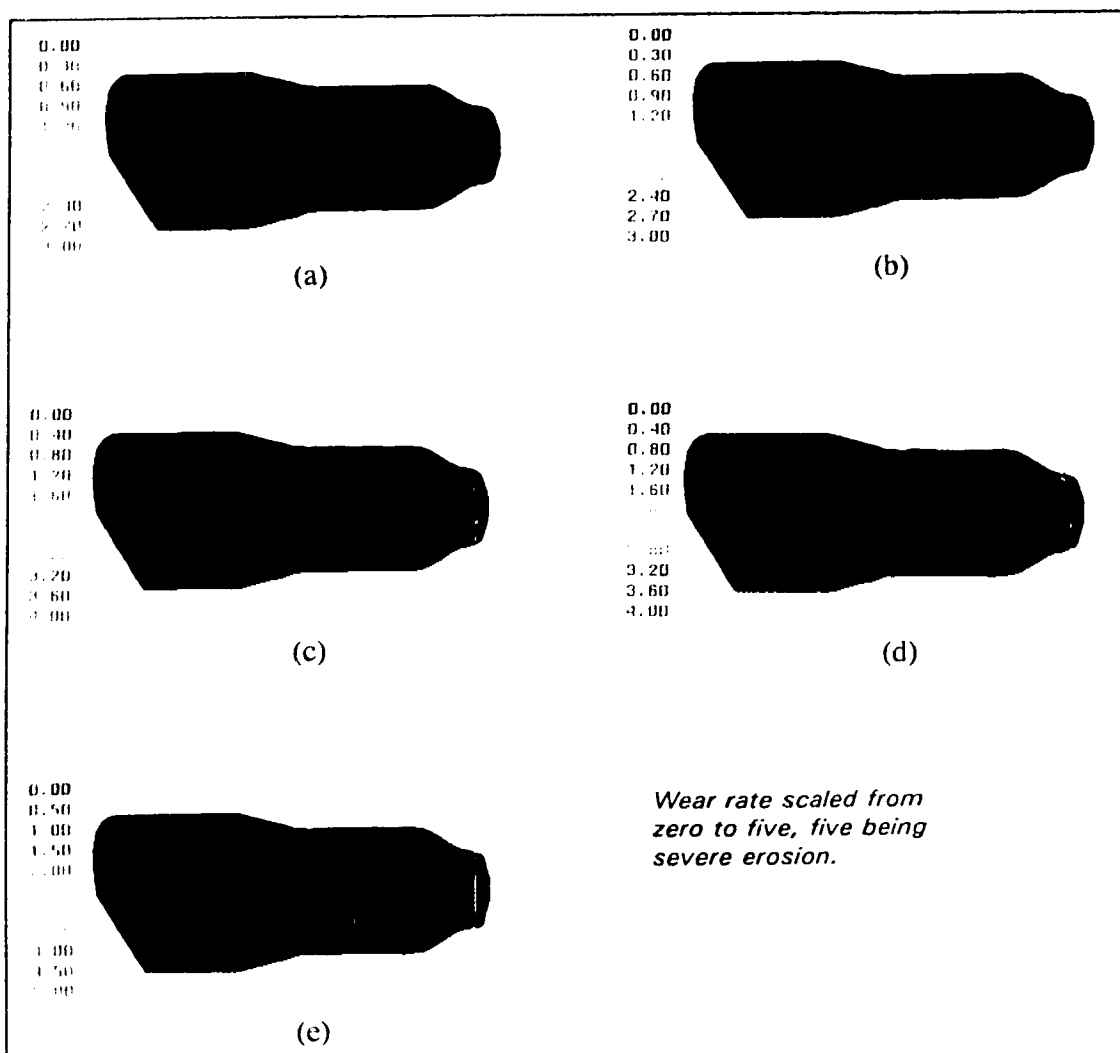


Figure 4.18. Comparison between predicted and actual wear patterns for the valve plug assembly. (a) 10 μm , (b) 20 μm , (c) 50 μm , (d) 100 μm , (e) Operational valve.

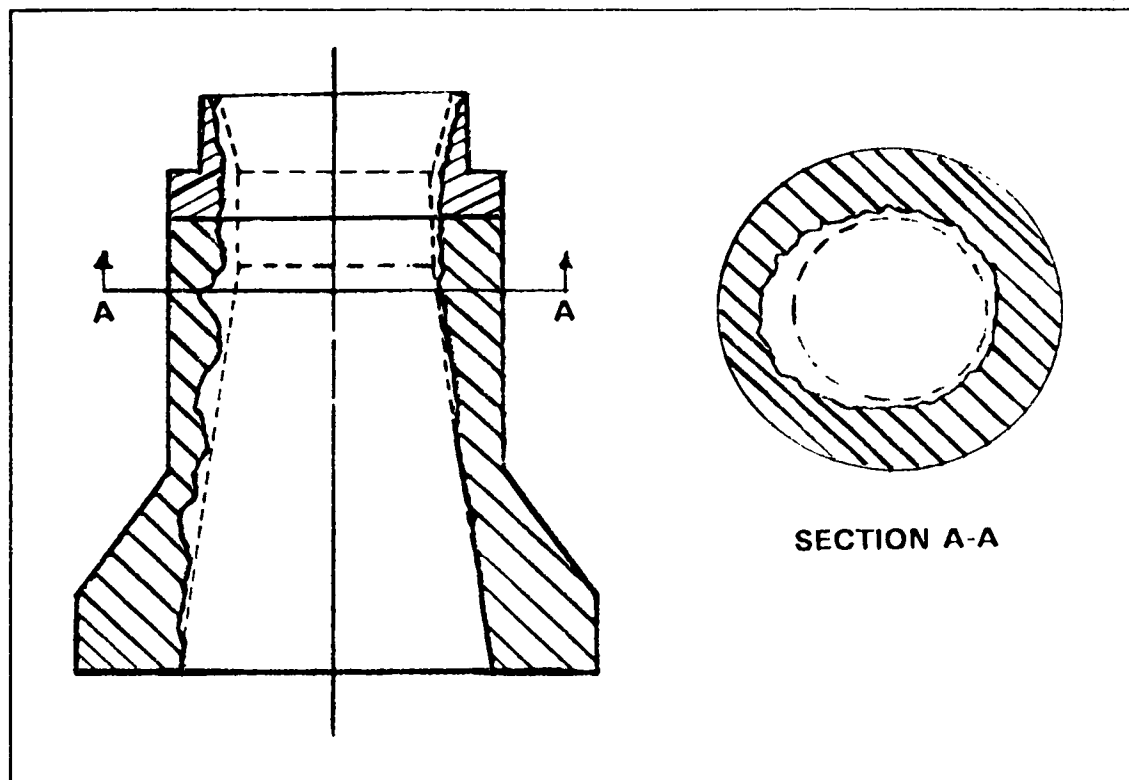


Figure 4.19. Schematic representation of erosion predominantly to one side of the seat rings. Dashed line represents contours of the new seat rings.

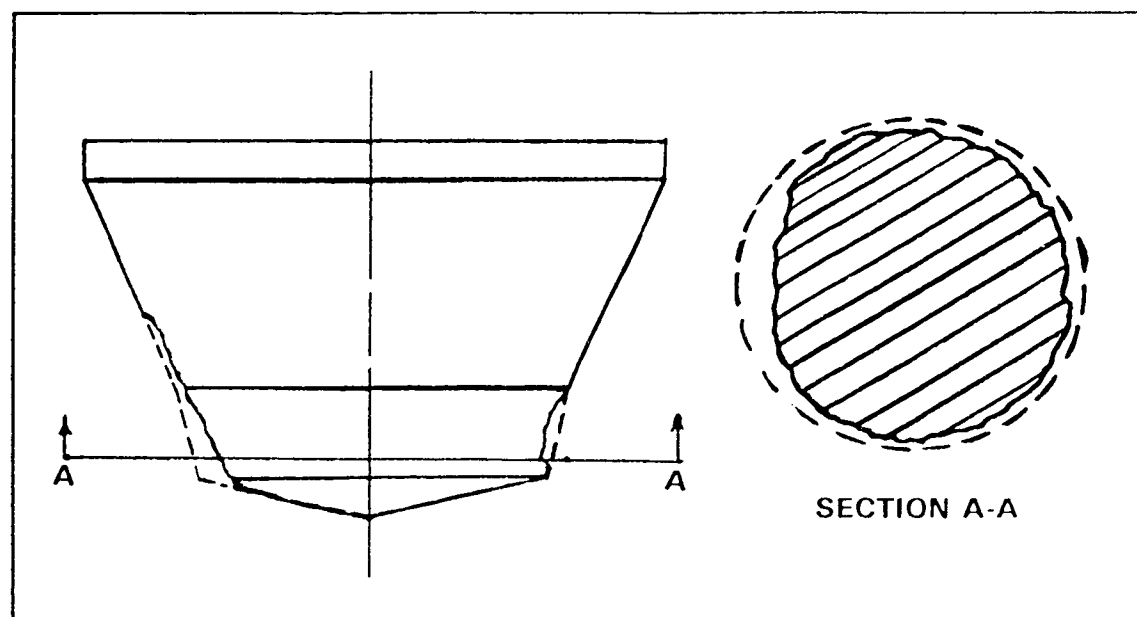


Figure 4.20. Schematic representation of erosion predominantly to one side of the valve tip. Dashed line represents contours of a new valve tip.

Chapter 5

5.1 Conclusions

The results of the erosion of a high pressure letdown valve can be summarized as follows.

- (1) The erosion prone areas of the valve tip, valve seat rings and valve's main body just above the top seat ring were qualitatively able to be predicted from the particle impact information of impact location, velocity, and angle.
- (2) Impact velocity and angle should aid in the selection of erosion resistant materials and help explain the good performance of some inserts.
- (3) This type of simulation should be a beneficial tool when making decisions regarding methods of erosion reduction by altering valve shapes, and sizes.
- (4) More quantitative results would be possible if experimental information was available for material constants in the empirical wear models.
- (5) The pressure drop across the valve could not be matched since the fluid downstream of the valve tip is likely a multiphase hydrocarbon, and possibly due to inadequacies of the $k-\epsilon$ turbulence model in an adverse pressure gradient

and recirculation zone.

- (6) The erosion rate by 50-100 μm particles overestimated the erosion while 10-20 μm particles were in better agreement with operational valve's erosion rates except for the bottom of the main body above the seat rings. This is not surprising since measurements by Stropki^{12,13} indicate that the average particle size is between 10-20 μm .

5.2 Suggestions for Further Work

A great deal of work remains to be done with this type of simulation before quantitative results are possible. The greatest numerical difficulty with CFDS-FLOW3D occurred with the particle tracking routines. A large percentage of particles were lost in the valve simply due to particles moving too slowly along the walls. If the particle tracking routines could be modified or rewritten to eliminate this problem, quantitative results should be possible. This was done by Benim et al³ in their simulation of erosion in turbocharger radial turbines.

Possible changes to the valve contours that should be modelled to investigate the potential to reduce erosion would be as follows: increase the size of the main body, lower the diffuser angle of the lower seat ring, and modify the shape of the valve tip and top seat ring.

Experimental work is required to get better constants for empirical wear models for the particular erodents and materials being eroded in this valve. Additionally, the affects of corrosion and cavitation should also be considered when modelling solid particle erosion in this geometry.

References

- 1) Grant, G. Tabakoff, W., "Erosion prediction in turbomachinery resulting from environmental solid particles", *Journal of Aircraft*, Vol. 12, No. 5, 471-478, 1975.
- 2) Beacher, B. Tabakoff, W. and Hamed, A., "Improved Particle Trajectory Calculations Through Turbomachinery Affected by Coal Ash Particles", *Trans. ASME, Jr. Eng. Power*, Vol. 104, No.1, P. 64, 1982.
- 3) Benim, A.C. and Neuhooff, H.G., "Analysis of Erosion Behaviour in a Turbocharger Radial Turbine", *Int. J. Numer. Methods Fluids*, Vol. 16, 259-285, 1993.
- 4) Ahmad, K. and Goulas, A., "On the Use of Particle Trajectories for the Prediction of Erosion in Slurry Pumps", *ASME-FED*, Vol. 38, 125-133, 1986.
- 5) Nesic, S. and Postlethwaite, J., "A predictive Model for Localized Erosion-Corrosion", *Corrosion*, 582-589, 1991.
- 6) Benchaita, M.T. "Erosion of a Two-Dimensional Channel Bend by a Solid-Liquid Stream", *Trans. CSME*, Vol. 9, No. 2, 98-104, 1985.
- 7) Dosanjh, S. and Humphrey, J.A.C., "The influence of Turbulence on Erosion by a Particle-Laden Fluid Jet", *Wear*, Vol. 102, 309-330, 1985.
- 8) Vaughan, N.D. Johnston, D.N. and Edge, K.A., "Numerical Simulation of Fluid Flow in Poppet Valves", *Proc. Inst. Mech. Engrs*, Vol. 206, No. 2, 119-127, 1992.
- 9) Burns, A.D. Jones, I.P. Kightley, J.R and Wilkes, N.S., *Harwell-FLOW3D Release 3.2 "User Manual, CFDS*, Harwell Laboratory, Abingdon, 1993.
- 10) Humphrey, J.A.C., "Fundamentals of Fluid Motion in Erosion by Solid Particle Impact", *Int. J. Heat and Fluid Flow*, Vol. 11, No. 3, 170-195, 1990.
- 11) Ottjes, J.A., "Digital Simulation of Pneumatic Particle Transport", *Chemical Engineering Science*, Vol. 33, 783-786, 1978.
- 12) Stropki, J.T., "Erosion Testing of Syncrude Bitumen and Once-Through Scrubber Bottoms", *Syncrude - Phase I Final Report*, Battelle Laboratories, Columbus Ohio, 1990. (For a Copy Contact Syncrude Research, Edmonton, Alberta)

- 13) Stropki, J.T., "Comparison of Erosion Resistance for Candidate Valve and Pump Materials", Syncrude -Phase II Final Report, Battelle Laboratories, Columbus Ohio, 1991. (For a Copy Contact Syncrude Research, Edmonton, Alberta)
- 14) Levy, A.V. and Chik, P., "The Effects of Erodent Composition and Shape on the Erosion of Steel", *Wear*, Vol. 89, 151-162, 1982.
- 15) Anand, K. Hovis, S.K. Conrad, H. and Scattergood, R.O., "Flux Effects in Solid Particle Erosion", *Wear*, Vol. 118, 243-257, 1987.
- 16) Liebhard, M. and Levy, A., "The Effect of Erodent Particle Characteristics on the Erosion of Metals", *Wear*, Vol. 151, 381-390, 1991.
- 17) Karimi, A. and Schmid, R.K., "Ripple Formation in Solid-Liquid Erosion", *Wear*, Vol. 156, 33-47, 1992.
- 18) Bitter, J.G.A., "A Study of Erosion Phenomena Part I", *Wear*, Vol. 6, 5-21, 1963.
- 19) Bitter, J.G.A., "A Study of Erosion Phenomena Part II", *Wear*, Vol. 6, 169-190, 1963.
- 20) Stack, M.M. Stott, F.H. and Wood, G.C., "Review of Mechanisms of Erosion-Corrosion of Alloys at Elevated Temperatures", *Wear*, Vol. 162-164, 706-712, 1993.
- 21) Finnie, I., "Erosion of Surfaces by Solid Particles", *Wear*, Vol. 3, 87-103, 1960.
- 22) Hutchings, I.M., "A Model for the Erosion of Metals by Spherical Particles at Normal Incidence", *Wear*, Vol. 70, 269-281, 1981.
- 23) Bergevin, K., "Effects of Slurry Velocity on the Mechanical and Electro-Chemical Components of Erosion-Corrosion in Vertical Pipes", M.S. Thesis, Univ. of Saskatchewan, Saskatoon, 1984.
- 24) Majumdar, S. and Sarajedini, A., "A Review of Solid Particle Erosion of Engineering Materials", ASME-PVP, Vol. 139, 79-86, 1988.
- 25) Neilson, J.H. and Gilchrist, A., "Erosion by a Stream of Solid Particles", *Wear*, Vol. 11, 111-122, 1968.
- 26) Wright, I.G. Shetty, D.K. and Clauer, A.H., "Erosion-Resistant Materials for Critical Areas of Coal Liquefaction and Coal Gasification Systems", *J. Materials for Energy Systems*, Vol. 6, No. 3, 172-183, 1984.

- 27) Anand, K. and Conrad, H., "Microstructure and Scaling Effects in the Damage of WC-Co Alloys by Single Impacts of Hard Particles", J. Materials Science, Vol. 23, 2931-2942, 1983.
- 28) Hockey, B.S. and Wiederhorn, S.M., Proc. 5th Int. Conf. Erosion by Liquid and Solid Impact, Cambridge Univ., UK, pp. 26, 1979.
- 29) Conrad, H. McCabe, D. and Sargent, G.A., "Effects of Microstructure on the Erosion of WC-Co Alloys", Science of Hard Materials, 775-796, 1983.
- 30) Evans, A.G. Gulden, M.E. and Rosenblatt, M., "Impacts Damage in Brittle Materials in the Elastic-Plastic Response Regime", Proc. R. Soc. Lond. A. Vol. 361, 343-365, 1978.
- 31) Conrad, H. Shin, Y. and Sargent, G.A., "Erosion of Sintered WC-Co Alloys", Specialty Steels & Hard Materials, 423-429, 1982.
- 32) Laugier, M.T., "Particulate Erosion of WC-Co Composites at Elevated Temperature", Proc. 7th Int. Conf. on Erosion by Liquid and Solid Impact, pp. 61, 1986.
- 33) Prinos, P. and Goulas, A., "Flow Characteristics in the Downstream Region of a Conical Diffuser", Int. J. for Numer. Method in Fluids, Vol. 15, 377-397, 1992.